A COMPUTATIONAL TOOL FOR NUMERICAL PREDICTION OF PRECISION GLASS MOLDING PROCESS

By

SHRIRAM PALANTHANDALAM MADAPUSI

A THESIS PRESENTED TO THE GRADUATE SCHOOL
OF THE UNIVERSITY OF FLORIDA IN PARTIAL FULFILLMENT
OF THE REQUIREMENTS FOR THE DEGREE OF
MASTER OF SCIENCE

UNIVERSITY OF FLORIDA

2009

To my parents, Sneha and Rimsha

ACKNOWLEDGMENTS

I would first like to thank my parents for their unconditional love and the unwavering support that they have showered on me ever since. My gratitude towards them cannot be expressed in words.

I cannot thank Dr. Kim enough for being my mentor through the course of my graduate studies. Under his guidance for 2 years, I have learnt a lot and have definitely become a better individual in terms of research aptitude and professionalism. Furthermore, his constant moral support and understanding with his students makes him really special.

To be a part of the MDO research group was an intellectually stimulating experience. I was exposed to a variety of academic topics in the group. I thank all the members of the MDO group and Dr. Haftka for the same.

I am thankful to Dr. Kumar and Dr. Chen for being on my committee and for their time.

I am grateful to Dr. Yazid Tomhe for his guidance during my internship at Moore Nanotechnology Systems.

I am really thankful to all my roommates over the years, especially Shubhendu, Rajesh and Anirudh for they filled the void of my family in Gainesville. Their love, understanding and support indeed made my stay in Gainesville pleasant.

For all the fun that I had away from work, I acknowledge a big thanks to all the members of group Sanagam, The. With them I was able to have some of the most cherished and memorable moments in my life during the past two years.

TABLE OF CONTENTS

LIST OF TABLES

LIST OF FIGURES

Abstract of Thesis Presented to the Graduate School
of the University of Florida in Partial Fulfillment of the
Requirements for the Degree of Master of Science

A COMPUTATIONAL TOOL FOR NUMERICAL PREDICTION OF PRECISION GLASS MOLDING PROCESS

By

Shriram Palanthandalam Madapusi

August 2009

Chair: Nam-Ho Kim
Major: Mechanical Engineering

There is an increasing use of optical lenses in many consumer products such as CD/DVD players and cellular camera phones. Currently, these lenses are molded using plastics in high volumes. However, there is a high demand for glass optics for their superior optical properties such as lesser aberration and lower birefringence over plastics. In general, precision glass optics is fabricated through diamond machining, grinding, and polishing. A potentially lower cost and faster method to produce glass optics is compression molding, which is not widely used. The primary reason is because of the development of residual stresses which deteriorates the optical properties of the lens like refractive indices etc. Also, it is difficult to obtain geometrically correct optics because the molding occurs at high temperatures (550 – 700 ˚C). The geometries of both glass and molds are deformed due to thermal expansion and the complex behavior of glass at higher temperatures, because of which it becomes difficult to predict the thermal contraction during the cooling process.

This research has been dedicated to develop a physics-based computation tool to treat and quantify each individual process that occurs in the molding process such as heating, compressing, and cooling, and hence be able to predict the residual stresses and the final geometry of the glass element. Eventually this tool can be used to design the optimum glass

molding process which would generate residual stresses within acceptable limits and design appropriate mold geometry that can yield the correct shape of the final glass optics.

CHAPTER 1
INTRODUCTION

Precision Asphere Optics

A lens in the most fundamental terms can be defined as an optical device which transmits and refracts the light incident on it, resulting in the convergence or the divergence of the light beam. The surface profile of the lens is a crucial characteristic that governs the performance of an optical lens. Lenses have since long been used in applications like magnifying glasses, binoculars, microscopes, telescopes etc. However, for other advanced applications like medical and military equipments, scientific testing devices, projectors, digital cameras etc. the surface accuracy and finish should be precise. These kinds of lenses which require highly precise surface profiles and finish are known as precision lenses.

Conventional lenses generally have either cylindrical or spherical profiles. These lenses are relatively easy to fabricate and design. However, these lenses have major drawbacks in their optical properties like spherical aberration, coma, astigmatism etc. which are detrimental to the applications of precision lenses (1). For example, spherical lenses cannot focus light to a single point resulting in what is known as spherical aberration. The lenses refract the ray of light striking at the edge of the lens more than they do at the center and hence distorting the image as shown in Figure 1-1. This problem is circumvented by having multiple arrays of lenses in a row which compensates for the error to finally obtain convergence at a single point. However, multiple arrays of lenses result in greater complexities like alignment, need of multiple lenses and an overall bulkier optical system. Figure 1-2 illustrates the use of an asphere lens to eliminate the need for multiple lenses in an optical system.

Asphere lenses have a profile which is neither completely cylindrical nor spherical. Its profile is mathematically expressed by what is known as the asphere equation. An Asphere lens

can consist of multiple segments hence giving more flexibility to design the lens profile. The segments can be asphere, flat, spherical etc. An axisymmetric asphere profile in a 2 dimensional x-z plane can be described by Equation 1-1

$$z = f(x) = \frac{c_v x^2}{1+\sqrt{1-(1+k)c_v^2 x^2}} + \sum_{i=1}^{n_a} A_i x^i \qquad 1\text{-}1$$

In Equation 1-1, c_v is the radius of curvature, k is the conic constant and A_i are known as the asphere constants with n_a specifying the number of constants, the maximum typically being up to 20. Figure 1-3 shows the profile that corresponds to an asphere equation of the above form.

Comparison between Glass and Plastic Lenses

Plastics lenses have certain advantages over glass lenses, most of them pertaining to physical properties. Plastic lenses are light weight and easy for mass production. Hence they find ample applications in common eye glasses. Plastic lenses however have poor optical properties and offer limited range of refractive index which varies greatly with temperature.

Glass lenses have always been the choice for optical applications. They have superior optical properties like transparency, wide range of refractive index etc. Glass lenses are more scratch and moisture resistant. The thermal expansion coefficient of a glass lens is less than that of a plastic lens by a factor of 1/60 – 1/120 (2). Hence in applications where a highly precise optical profile is desired for performance, temperature dependent properties are undesirable.

Because of the superior optical properties possessed by glass lenses, they are invariably preferred in precision and semi-precision optical systems.

Conventional Asphere Glass Lens Manufacturing

The conventional optical manufacturing process is usually preformed by an abrasive process followed by surface polishing (3). The first step is a rough shaping of the aspherical shape on the surface of the glass by grinding with loose or bound abrasives. The machining is

performed using silicon carbide (SiC) or diamond grinding wheels. Glass being brittle, bulk of the material is removed by brittle fracture which leaves a rough surface. The second step is a crucial step where the roughness and the shape accuracy of the surface is improved to the desired precision levels. This process provides satisfactory curve conformance in case of spherical lenses (4). However, for asphere lenses, one needs a more sophisticated process for the polishing process because of the complexity and the precision of the asphere profile involved. Machine error inevitably poses obstacles when one is trying to obtain very precise complex curves. Furthermore, these processes require continuous surface evaluation and correction. This is a time consuming iterative process despite the advances in modern CNC deterministic grinders and polishers. It is typical to have grinding and polishing runtimes of 2-3 hours per surface.

There are a few modern commercial sophisticated polishing processes that are used for manufacturing asphere lenses. One of them is the magnetorheological finishing in which a carrier fluid (generally oil) contains a suspension of magnetic particles. The viscosity of the fluid varies greatly with the change in magnetic field. With the help of an electromagnet, the fluid's ability to transmit force can be controlled precisely and this very force can be used to polish glass surfaces to a great precision (5). Another method is known as the ion beam finishing method in which individual atoms in an ion beam are used to ablate a target (6). Other similar processes used in manufacturing asphere lenses are precessions grinding, fresh feed polishing, precision grinding etc.

However these processes prove expensive for large or even medium volume production due to the overall complexity of these processes (7). In addition, these processes cause environmental threats due to their extensive use of fluids like polishing slurries and grinding

fluids. Concerns regarding health hazards also arise due to the glass debris, especially that of glasses with high lead concentration.

Compression Molding of Asphere Lenses

Due to the limitations of the conventional asphere lens manufacturing process, and due to the high expense incurred, an attractive emerging technique to manufacture asphere precision lenses is the compression molding process. A lot of research has been done on developing the compression molding method for asphere lenses (8) (9).

A general compression glass molding process is described in the following way:

A cylindrical or an elliptical glass gob is mounted between two molds having desired profile of the final lens shape. The entire setup consisting of the molds and the glass is heated to a temperature above the glass transition temperature. Glass being a vitreous material does not change from solid to liquid directly when heated. It essentially behaves as a viscoelastic material at temperatures near the glass transition temperature. The viscosity of glass generally lies in the range of $10^{10} – 10^{9}$ Pa-secs (10) and glass is soft enough in this range to be molded easily to the desired shape. The molds are pressed on the soft glass to result in the desired glass profile and the setup is brought back to room temperature in a controlled fashion.

During the heating process, which is generally done using infrared lamps, the glass and the molds are maintained at a steady state temperature so as to ensure that the glass and the molds have a uniform temperature distribution. With the temperature being constant, the molds are pressed to deform the glass to the desired shape. Initially the glass is cooled in a controlled manner by purging the system with Nitrogen gas. The heat is removed from the molds by convective heat transfer and the molded glass lens loses heat to the colder molds by interfacial heat transfer or heat conduction. During this stage, a relatively smaller compressive load is

maintained to ensure the final alignment of the lens for the proper shape and to prevent excessive shrinkage of the lens during cooling.

Advantages and Benefits

Lenses produced by compression molding process have many desirable advantages over conventional manufacturing process. This method produces a near final shape of the lens and doesn't require any further finishing. It is a faster method because of the minimal amount of processes required as compared to the conventional machining process. For the same reasons, compression glass molding approach is much cheaper than the conventional manufacturing process which uses techniques like magnetorheological finishing, ion beam polishing etc. which are very expensive. Figure 1-4 illustrates the comparison between the two approaches.

Compression molding process is also environment friendly as it doesn't require any polishing fluids or grinding slurries and doesn't leave any glass debris that needs to be disposed off with care. Most asphere glass lenses contain hazardous elements like lead and arsenic; hence the disposal of the manufacturing glass debris needs to be done with care.

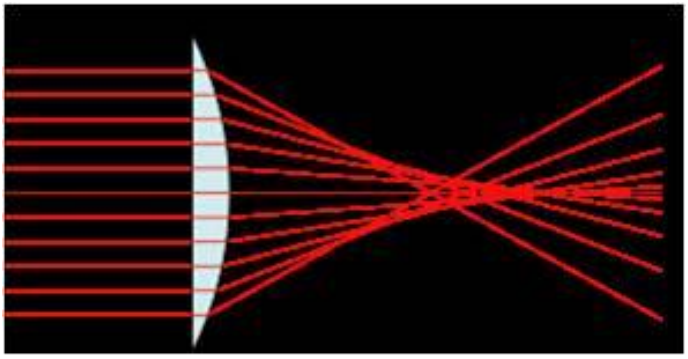

Figure 1-1. Spherical aberration error in a spherical lens

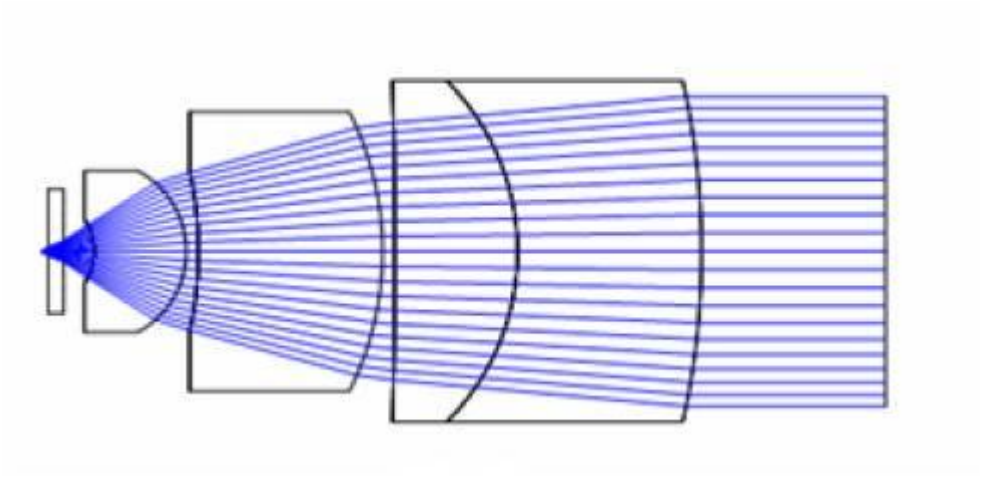

A

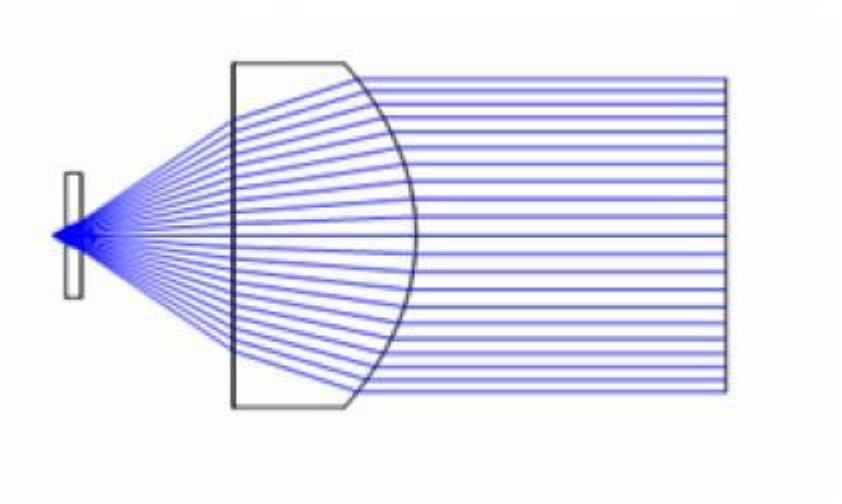

B

Figure 1-2. Comparison between use of asphere and spherical/cylindrical lenses. A) Use of multiple spherical/cylindrical arrays, B) Use of single asphere lens to achieve the same effect

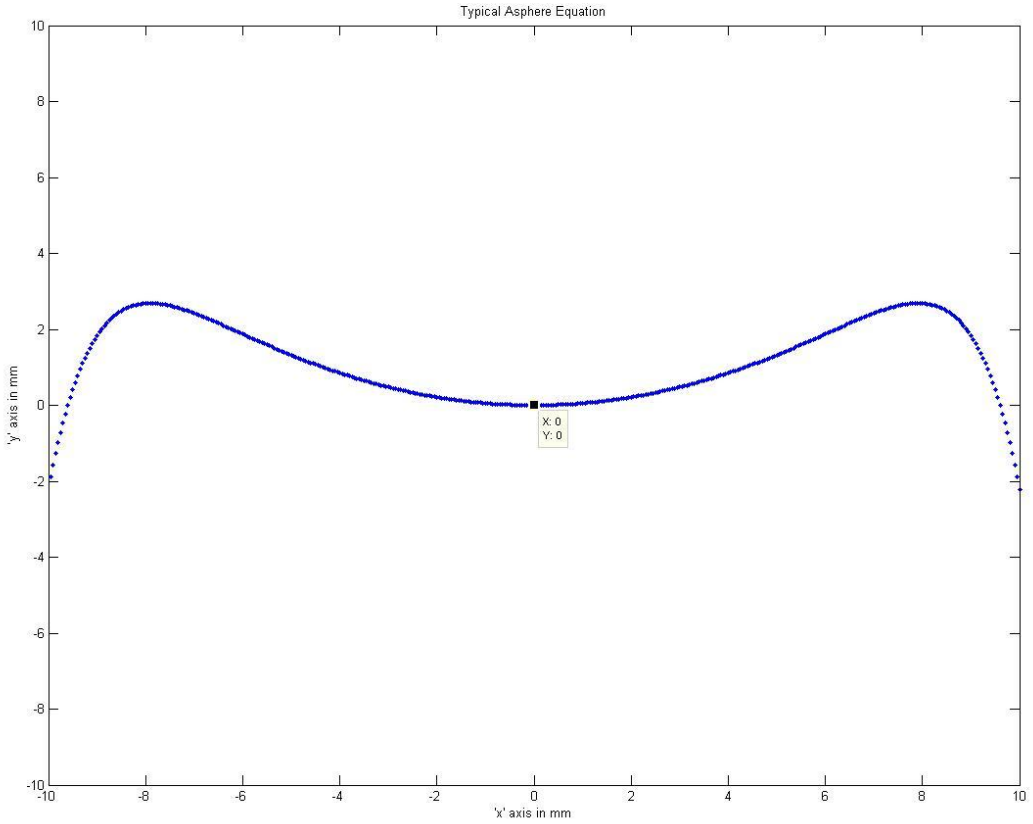

Figure 1-3. Plot showing the profile of a typical asphere curve. (the axes units are in ‘mm’)

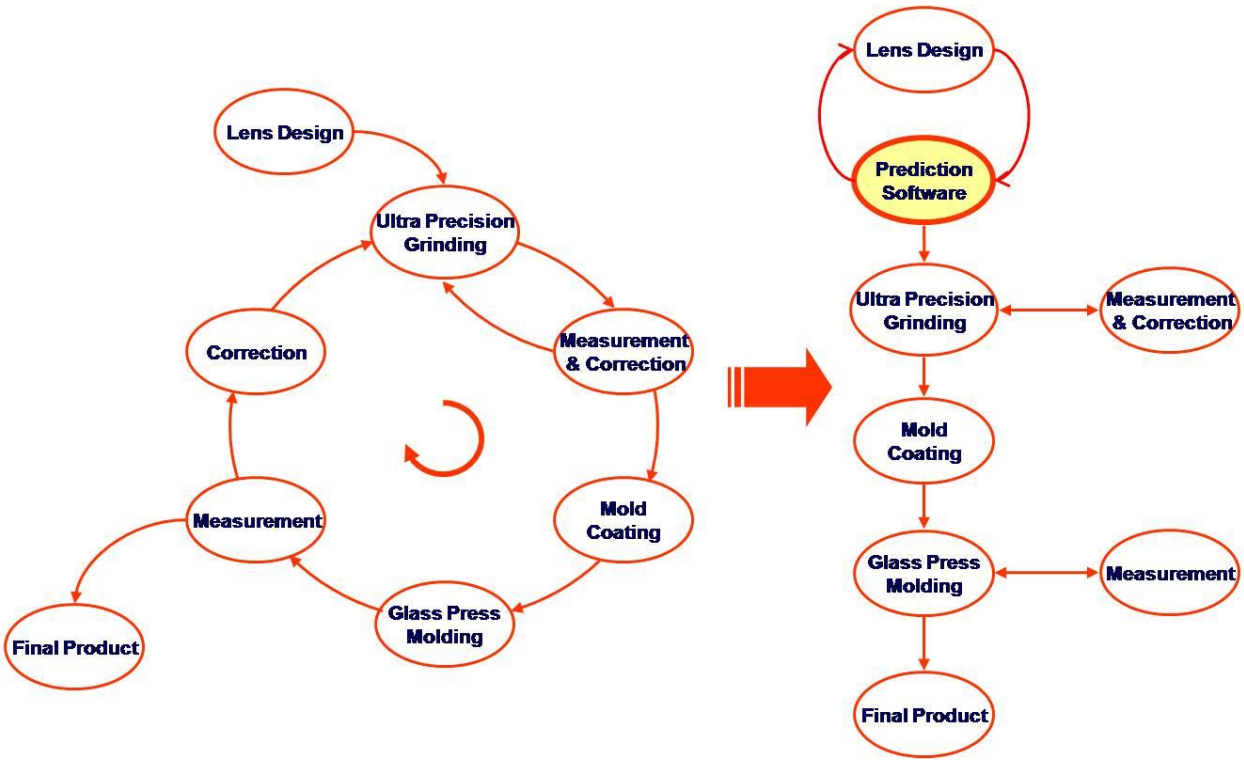

Figure 1-4. Comparison of glass molding processes without and with the use of a numerical tool.

CHAPTER 2
RESEARCH OBJECTIVES

Challenges

Technology to produce molded optics exists commercially, but is not widely used because of the challenges that entail with the process.

Firstly, the most crucial process is the cooling process in which glass undergoes a second order phase transition from a viscoelastic solid to an amorphous solid at room temperature. This leads to residual stresses in glass which affect its optical properties like refractive index and the final shape of the lens due to shrinkage. This final profile of the lens and the need for accuracy in this profile is vital in case of precision lenses. Residual stresses affect optical properties of glass and hence it is desired that the residual stresses be at a minimum value at the end of the molding process. The accumulation of residual stresses depends on the cooling rate. It is therefore important to predict and control the cooling rate so that the residual stresses are acceptable for optical performance of the lens.

Secondly, it is a challenge to design molds that will yield geometrically correct optics at the end of the molding process. This arises because of the fact that during the heating of the molds and glass, the profiles of the molds change due to thermal expansion and they recover their shapes at the end of cooling.

Furthermore, glass behaves like an amorphous elastic solid at room temperature and behaves like a viscoelastic solid at higher temperatures. At these temperatures the material properties of glass are highly dependent on temperature and time and hence it is difficult to model the material behavior.

Hence, even though the glass molding process itself is relatively simple, designing the molding process as a whole to result in a predicted glass optic can be difficult. There is a need to

quantitatively predict the glass molding process which would aid us to design the glass molding process.

Objectives

Although compression molding of glass is an attractive alternative to produce cost effective and large scale production of precision optical element, the inherent technical challenges associated with it have hindered the process being used widely in the industry.

Numerical simulation of the compression molding process would help in predicting the molding process and can aid in designing the molding process for manufacturing of desired optical elements. Using commercially available software, one can model the process as an all in one brute force simulation, without a complete understanding of the underlying physics of the process. Commercial software is not customized for glass molding applications. Accordingly, computational resources can be wasted for non-significant part of the model, while critical parts may not have enough level of details.

Thus the overall objective of this research is to understand the basic underlying physics of the glass molding process and be able to delineate the vital process responsible for the final product quality. Valid engineering assumptions are made and individual processes (such as heating, pressing, cooling etc.) are analyzed separately in a preliminary attempt to develop a customized numerical simulation tool for predicting the glass molding process. The finite linear/nonlinear element methods are implemented for the simulation.

More specific research objective of this work is to develop a relatively simple physics-based numerical method but yet accurate enough to model a compression glass molding process for manufacturing process, predict the final shape of the glass element at the end of the molding process, quantitative analysis of glass material properties at higher temperature and to predict the critically important residual stresses at the end of the molding process.

Purpose and Implications of Research

The fundamental purpose of the research is to understand the glass molding process and develop a relatively simple computational model to predict the same.

The implications of developing such a tool would be prediction of the glass molding process and help in designing the process in a way that would result in the final desired optical element. It would help in prediction of the residual stresses and hence in the optimum design of the process parameters of the molding process.

CHAPTER 3
LITERATURE SURVEY

Because of increasing demand for high quality optical glass components such as aspherical lenses, the need to develop an efficient and economic production process is significant to the optics industry. High precision glass molding technologies have tremendous potential to fulfill the needs of economic complex shaped optical components.

Due to the complexities involved in a glass molding process and the precision that needs to be achieved, the glass molding process chain is driven by iterative cycles between mold designs, lens profile, residual stresses etc. Multiple cycles are necessary to reach the final accuracy of the lens profile and to determine the optimum cooling rate to have residual stresses within acceptable limits. The process design and optimization work related to the glass molding process is performed by trial and error and using iterative procedures. Numerical simulation of the glass molding process can help to predict the final profile of the lens and most importantly predict the residual stresses at the end of the process.

Although technologies for designing machines that perform the glass molding process have been developed significantly, limited work has been established in the field of numerical modeling of the glass molding process. This can be attributed to some major challenges such as modeling the material model of glass which is dependent on both time and temperature, time and temperature dependent boundary conditions, large deformations and contact phenomena, which in totality make the analysis highly nonlinear. It is possible to model all these characteristics using commercial software, but it would be an expensive alternative – monetarily and computationally.

Sadegh et al. (11) developed a finite element code to simulate the glass container forming process. The analysis involved a coupled thermomechanical systems in two dimensions with

large deformation and time dependent boundary conditions. The results showed the position of the glass material and the temperature distribution in glass during various stages of the forming process.

Arvind et al. (12) modeled the development of residual stresses that are developed in polymer films bonded to elastic substrates using viscoelasticity. The authors also showed that with an elastic material model, the residual stresses cannot be captured. Hence a time dependent stress analysis is necessary. An analysis on a polymer film, with elastic substrates subjected to a thermal cycle, was performed and the results showed stress reversals for the peel stresses. These explain failure modes not expected by an elastic analysis.

Simon et al. (13) investigated the role of structural relaxation in viscoelastic materials and in the evolution of free strain and stress relaxation times. They compared numerical and analytical results of a glass sample, bonded to metal substrate, subjected to a hysteresis loop and achieved comparable results. Cuong et al. (14) simulated the annealing process of glass bottles using theory of viscoelasticity and implemented the Narayanaswamy model for structural relaxation and performed the analysis in ANSYS. The maximum cooling stresses were located in the transition range. For the optimum annealing process, the authors emphasized the importance of the soaking process i.e. to ensure that the whole glass sample is at a uniform temperature. The development of the residual stresses is dependent on the cooling rate during the transition phase of glass, and rapid cooling can be performed once the temperature is below the transition phase.

Hoque et al. (15) applied a commercial finite element software (DEFORM 3D) to simulate the glass pressing in a television panel forming process. A glass gob at 1000 ºC is pressed between the plunger and the mold. The glass material was modeled assuming glass to be a Newtonian fluid in that phase and temperature dependent viscosity was implemented. The

authors compared the model predictions with experimental measurements under production conditions and obtained reasonable results with differences of about 5-10%.

Soules et al. (16) implemented a commercial FEM program, MARC, to predict the thermal residual stresses in three problems: sandwich seal, bead seal under the conditions of uniform cooling and reheating, and a glass plate undergoing tempering. In the glass plate example, the cooling was an unconstrained cooling but they were able to show the development of residual stresses due to the viscoelastic behavior of glass. This is otherwise not possible with an elastic material modeling of the glass sample. The tempered glass was cooled from an initial temperature of 570 ºC to 20 ºC by forced convection on both sides. Residual stresses were generated because of the phase change of glass with cooling and due to the non-uniform cooling. The viscoelastic theory governing the stress and structural relaxation effects was modeled according to the Narayanaswamy model. A good agreement was obtained between the numerical simulations, analytical results and experimentally measured stress values using the photoelasticity method. The author had proposed that using the numerical development, it is possible to predict the residual stresses that arise in materials which exhibit viscoelasticity.

Jain et al. (17) demonstrated that it is possible to numerically model the glass molding process using commercial finite element software like DEFORM 3D and MSC Marc. Since DEFORM 3D doesn't have the capacity to model the phenomena of structural relaxation, the authors performed the analysis assuming glass as elastic material during the cooling phase. The authors were able to capture reasonably correct profile at the end of the process but could not predict the residual stresses. However, they concluded that predicting the glass molding process can be improved with an enhanced model and can be made computationally economical with engineering assumptions.

A lot of research has been performed on the numerical modeling of glass forming and tempering process. However, the author of this thesis has not seen a dedicated development of a computational tool to model the physics and simulate the glass molding process. In this preliminary work, the author has attempted to develop a numerical tool for glass molding process by understanding the physics of the glass molding process and modeling the process with engineering assumptions so as to achieve computational simplicity and yet develop a good model for manufacturing processes.

CHAPTER 4
FUNDAMENTALS OF GLASS RHEOLOGY

Viscoelasticity

Viscoelasticity is the time dependent response of a material to a mechanical load. The classical one dimensional Hooke's law for elastic materials can be expressed by Equation 4-1 relating the stress and the strain through Young's modulus. The response is almost instantaneous, or to be more precise, the response occurs at the speed of sound.

$$\sigma = E\varepsilon \tag{4-1}$$

For an ideal Newtonian fluid, the shear stress is related to the rate of application of strain as described in Equation 4-2.

$$\sigma = \eta \frac{d\varepsilon}{dt} \tag{4-2}$$

where, η is the viscosity of the fluid.

A viscoelastic material exhibits a response which is a combination of elastic response and viscous response. Hence there is an instantaneous response of a viscoelastic material to an applied mechanical load, followed by a time dependent viscous response. At molecular level, when stress is applied to a viscoelastic material like glass or polymer, part of the long material chain change composition. This movement or rearrangement is known as creep. The material still remains as a solid material while these rearrangements happen in order to accompany the applied stress. This generates a back stress in the solid, and when the applied stress is taken away the back stress causes the material to return to its original form. Hence, the material creeps due to its viscosity (hence the prefix viscous) and as it eventually returns to its original form, the suffix elasticity (18)

Viscoelastic material behavior can be represented phenomenologically by a combination of dashpots and springs. Many such models have been developed, for instance the Kelvin model, Voight model, Maxwell model etc. The detailed formulation of these models are given in (19).

The most general formulation to describe the viscoelastic behavior is the generalized Maxwell model which has been used throughout this text.

Figure 4-1 shows what is known as the standard linear model. It consists of a Hookean spring placed in parallel with another spring and dashpot in series (Maxwell Model). In this arrangement, the Maxwell arm and the parallel spring G_∞ experience the same strain, and the total stress σ is the sum of the stresses in each arm as in Equation 4-3:

$$\sigma = \sigma_v + \sigma_\infty \tag{4-3}$$

where σ_v denotes the viscous stress in the Maxwell arm and σ_∞ is the stress acting on the spring with spring constant G_∞. If the total strain is ε, then as shown in Figure 4-1, by equilibrium we have:

$$\sigma = G_\infty \varepsilon + \sigma_v \tag{4-4}$$

Also, by using Equation 4-2 and the linearity of the elastic stress-strain response, we have

$$\sigma_v = \eta \frac{d\alpha}{dt} = G(\varepsilon - \alpha) \tag{4-5}$$

where, α is the strain induced in the dashpot and η is the viscosity of the dashpot. We define the constants in Equation 4-6 for convenience:

$$\begin{aligned} G_0 &:= G_\infty + G \\ \tau &:= \eta / G \end{aligned} \tag{4-6}$$

G_0 can be termed as the initial stiffness of the system at t=0 and τ can be defined as the relaxation time of the system.

Equation 4-4 and Equation 4-5 along with the use of constants defined in Equation 4-6 lead to the constitutive equation for the stress response as given in Equation 4-7 and Equation 4-8.

$$\sigma = G_0\varepsilon - G\alpha \tag{4-7}$$

$$\frac{d\alpha}{dt} + \frac{1}{\tau}\alpha = \frac{1}{\tau}\varepsilon \tag{4-8}$$

The stress response can be formulated in terms of a convolution integral by eliminating the internal variable α(t) from Equation 4-7 and Equation 4-8, as shown in Equation 4-9 (20):

$$\sigma(t) = \int_0^t G(t-s)\frac{d\varepsilon(s)}{ds}ds \tag{4-9}$$

where, s is known as the dummy variable, pseudo time or past time, and G(t-s) is called the relaxation modulus which is expressed by Equation 4-10:

$$G(t) = G_\infty + G\exp(-t/\tau) \tag{4-10}$$

The standard linear model can be easily generalized to include an arbitrary number of Maxwell elements arranged in parallel – which is known as the generalized Maxwell model as shown in Figure 4-2. A real viscoelastic material does not conform to the response as predicted by the standard linear model but instead conforms to the generalized Maxwell model which leads to a distribution of relaxation times. This in turn produces a relaxation spread over a much longer time than can be modeled accurately with a single relaxation time. This model has been adopted throughout this text to model viscoelasticity.

Generalizing the stress response for the model shown in Figure 4-2 by the same procedure, the stress response can be expressed by Equation 4-11 and Equation 4-12:

$$\sigma(t) = \int_0^t G(t-s)\frac{d\varepsilon(s)}{ds}ds \tag{4-11}$$

where

$$G(t) = G_\infty + \sum_0^N G_i \exp(-t/\tau_i) \quad \text{4-12}$$

where N is the number of Maxwell arms or Maxwell elements.

Stress Relaxation

An important phenomenon exhibited by viscoelastic materials is stress relaxation which essentially is how the material relieves stress with time because of the exponentially decaying modulus as shown in Equation 4-12. From Equation 4-12 we can see that at time=0 we have the shear modulus as given by Equation 4-13:

$$G(0) = G_0 = G_\infty + \sum_{i=1}^N G_i \quad \text{4-13}$$

which is the instantaneous modulus (elastic equivalent). After a long time has passed by i.e. at an infinite time we have the shear modulus at infinite time give by Equation 4-14:

$$G(\infty) = G_\infty + \lim_{t\to\infty} \sum_{i=1}^N G_i \exp(-t/\tau_i) = G_\infty \quad \text{4-14}$$

which is the constant modulus that remains after an infinite time. If G_∞ is set to zero, it would mean that the modulus relaxes completely to zero and hence the stress completely relaxes to zero. Figure 4-3 illustrates the exponential decay of the modulus with time.

Figure 4-4 illustrates the stress response of a material like glass when subjected to an instantaneous strain ε_0 at time t_0. This is a 1 dimensional response as the applied strain is uniaxial. The important parameter governing the relaxation phenomena in viscoelastic materials is the relaxation time τ, defined as $\frac{\eta}{G}$ where η is the viscosity and G is the elastic modulus and the unit of relaxation time being [second]. Solids possess a very high viscosity, of the order of 1E12 Pa.s or more and hence do not display any noticeable flow in response to shear stress. On the other hand liquids have viscosity of the order of 1E-4 Pa.s due to which they cannot support

any shear stress. Viscoelastic materials possess a viscosity which lies in between those of pure solid and liquids. The following chapter discusses the viscosity and relaxation times of a viscoelastic material in more detail.

The Glass Transition

Glasses are amorphous solids at room temperature and exhibit interesting state transformations with change in temperature, unlike crystalline materials. Crystalline materials behave like ice, going directly from solid to liquid state when heated at the melting point. Glasses on the other hand are vitreous materials which behave more like plastic when heated. Their viscosity progressively decreases with increase in temperature, and at certain temperatures the viscosity of glass is ideal to duplicate precisely the surface of a mold by compression molding process.

More specifically, the glass transition is a pseudo second order phase transition in which a supercooled melt yields, on cooling, a glassy structure and exhibits properties similar to those of crystalline materials. A second order phase transition is a transition of state which has no associated latent heat. It is a continuous phase transition unlike first order phase transition where the state of a material remains constant until the latent heat associated with it is absorbed, following which phase transition takes place (21).

The glass transition is a region of temperature in which the rearrangements occur at a molecular level to attain equilibrium on a scale of perceivable time of the order of minutes or hours and hence the change of properties occur at a rate that is easily observed. When subjected to mechanical load in the region, time dependent change in dimensions results, which was outlined in the previous stress relaxation topic. If a glass in the transition region is subjected to a sudden change in temperature, time dependent change in properties (like volume, density etc.) occurs which is known as structural relaxation which is outlined in the subsequent topic.

Figure 4-5 illustrates the change in specific volume of a glass cooled through the transition region. In the liquid state, the viscosity of glass is so low that equilibrium with a step change in temperature is attained almost instantaneously. As the temperature is further lowered, the viscosity of the liquid increases and so does the time taken to attain equilibrium. This region of temperature is where the curve departs from the equilibrium curve as shown in region BC. At C the viscosity of glass is so high that the internal structure has essentially frozen into a glassy state. The region BC which corresponds to a state between the liquid and solid is called the transition range where the approach to equilibrium takes a finite time which can be observed experimentally. The transition temperature can be defined as the point at the center of the transition region which has the greatest curvature in V (T) (22). The slope of the curve (which is the measure of the expansion coefficient) changes from a higher value in the liquid state to a lower value in the solid state at the transition temperature as shown in Figure 4-6.

Figure 4-7 shows the trend of variation of viscosity of glass with temperature (23). At a very high temperature, quite above the melting temperature, the viscosity is very low - of the order of 1E0 – 1E4 dPa.s (1dPa.s = 10 Pa.s). During the cooling of the melt, the viscosity of the glass constantly increases as shown in Figure 4-7. When the viscosity reaches to the order of 1E4 – 1E13 dPa.s, the transition from a flowing, almost liquid like state, to a more plastic state can be observed. In glass molding process, the appropriate molding temperature would be the one with which the viscosity would decrease to the order of 1E7.6 – 1E9 dPa.s (24). At these temperatures, the viscosity of glass is low enough to dissipate stresses due to mechanical deformation of the order of milliseconds. Therefore, the stresses that arise from pressing are negligible. With a viscosity above 1E9 dPa.s, the viscosity becomes increasingly time dependent. With further increase in viscosity (or decrease of temperature) the time taken to attain structural

equilibrium is so large that for practical purposes the structure can be deemed as solidified or frozen.

Structural Relaxation

As outlined in the previous topic, structural relaxation is the phenomenon of time dependent change of a property, like a volume, when a viscoelastic material, like glass, is subjected to a sudden step change in temperature.

Suppose a viscoelastic material is at equilibrium at temperature T_1 which is suddenly cooled to temperature T_2, then the properties will change as shown in Figure 4-8. The instantaneous change in volume is characterized by α_g which is the coefficient of thermal expansion at the glassy state and the total change after equilibrium corresponds to α_l which is the coefficient of thermal expansion at the liquid state (25).

In the transition region, the response of a property to a small change in temperature from T_1 to T_2 is defined by the response function $M_v(t)$ given in Equation 4-14 as defined by (26).

$$M_v(t) = \frac{V(t) - V_2(\infty)}{V_2(0) - V_2(\infty)} = \frac{T_f(t) - T_2}{T_1 - T_2} \qquad 4\text{-}15$$

where the subscripts 0 and ∞ represent the instantaneous and long term values of volume (V), following the step temperature change. This function represents the fraction of the volume change that has not yet occurred.

The quantity T_f is defined as fictive temperature – the actual temperature of an equilibrium state that corresponds to the given non-equilibrium state. Hence if a liquid were equilibrated at T_f (T_1) and then instantaneously cooled to T_1, it would change along the line with slope α_g as no structural rearrangement would occur. The fictive temperature T_f is found by extrapolating a line from $V(T_i)$ with a slope α_g to intersect a line from $V(T_0)$ with slope α_l as illustrated in Figure 4-9. The experimentally measured shape of the response function is described by Equation 4-16 (27).

$$M_v(t) = \exp\left[-\left(t/\tau_v\right)^b\right] \quad \text{4-16}$$

where b is a phenomenological parameter whose value lies between 0 and 1 and is typically equal to 0.5 and τ_v is the structural relaxation time. Alternatively, the experimental data can be fitted more accurately by using a spectrum of relaxation times and weights similar to the Maxwell model as expressed in Equation 4-17

$$M_v(t) = \sum_{i=1}^{N} w_i \exp\left(-t/\tau_{vi}\right) \quad \text{4-17}$$

where each w_i corresponds to the weight associated with each i^{th} component and $\sum w_i = 1$.

These structural relaxation times and stress relaxation times as discussed earlier are strongly temperature dependent. In order to estimate the variation of these quantities with temperature, we assume glasses to exhibit thermorheologically simple behavior. It has been established that most of the inorganic glasses exhibit this phenomenon of thermorheological simplicity (28). The following topic addresses the temperature dependence of these quantities.

Thermorheological Simplicity

The structural and stress relaxation times vary significantly with change in temperature. However it has been established that most oxide glasses exhibit a convenient and predictable behavior with temperature change, called thermorheological simplicity.

In general, relaxation times increase rapidly with increase in temperature. For example, if we apply a constant uniaxial stress and note the decay of stress with time, the relaxation function which is a measure of the decay of stress given as $G(t) = \dfrac{\sigma_1(t)}{\sigma_1(0)}$ will vary with temperature as shown in Figure 4-10. However, if the relaxation curves are plotted against $\log(t)$, the curves are identical in shape, but shifted along the abscissa as shown in Figure 4-11 (29). The stress

relaxation curves can be shifted along the abscissa to superimpose them to a single convenient temperature known as reference temperature denoted by T_{ref} and incorporate the temperature dependence into a new time variable known as the reduced time, ψ as given in Equation 4-18

$$\psi = \int_0^t \frac{\tau_{ref}}{\tau\left(T(s)\right)} ds \qquad 4\text{-}18$$

where, τ_{ref} is the relaxation time measured at a suitable reference temperature. Hence Equation 4-17 now takes the form of Equation 4-19:

$$M_v(\psi) = \sum_{i=1}^{N} w_i \exp\left(-\psi / \tau_{vi}\right) \qquad 4\text{-}19$$

Furthermore, the relaxation times depend not only on temperature, but also on thermal history (30). Hence the relaxation times τ at any given time and temperature can be calculated using the model proposed by Narayanaswamy (26), using Equation 4-20

$$\tau = \tau_{ref} . \exp\left\{-\frac{H}{R}\left(\frac{1}{T_{ref}} - \frac{x}{T(t)} - \frac{(1-x)}{T_f(t)}\right)\right\} \qquad 4\text{-}20$$

where, T(t) is the current temperature, $T_f(t)$ is the fictive temperature associated with the current temperature and R is the universal gas constant H and x are considered to be phenomenological parameters for the purposes of this research with x typically being $0 < x < 1$. At temperatures above the glass transition temperature $T_f \simeq T$ and at lower temperatures where glass has essentially frozen into a solid, the fictive temperature T_f becomes a constant with a value equal to the glass transition temperature.

Calculation of Fictive Temperature: The fictive temperature which was discussed in the previous topic can be calculated by solving Equation 4-15, given the form of response function as in Equation 4-17 as a function of temperature and time (or reduced time) by using the

Boltzmann superposition principle and integrating over the thermal history of the sample which is given in Equation 4-21 (26) **.**

$$T_f(t) = T(t) - \int_0^t M_v\left(\psi(t) - \psi(s)\right)\frac{dT}{ds}\,ds \qquad 4\text{-}21$$

where, M_v is the response function as given in Equation 4-17 and s is the pseudo time or dummy time variable.

The fictive temperature can be calculated more efficiently for numerical implementation as proposed by Markovsky and Soules. The authors developed an algorithm to calculate the fictive temperatures by using the differential form of Equation 4-21 and assigned initial partial values of fictive temperatures and numerically integrated during a transient analysis using a stable implicit scheme. Further details are outlined in Chapter 7 where the numerical implementation of the molding process is discussed.

Identification of Material Parameters

As discussed in the previous sections, the viscoelastic properties of glass (viscosity or relaxation time) are strongly temperature dependent and hence are evaluated at a suitable reference temperature.

There are several methods to evaluate the viscoelastic properties of glass. The most common method is to fit the experimental data with analytical or mathematical constitutive model using method of nonlinear regression analysis or be the method of least squares (31). Creep and stress relaxation tests are the most commonly used methods to determine the viscoelastic properties of materials like glass etc. In these tests, instantaneous strain (or displacement) or stress (or force) is applied and the corresponding decay of the other quantity is noted. For example in a creep test, a sudden force is applied and the increase in strain is noted. However, because of machine limitations for applying instantaneous forces or displacements, the

application is not truly instantaneous and might be significant in case of some particular machines. The response during the period of loading is typically ignored and the data obtained from the state of constant strain or stress is used to determine the material properties. This further introduces additional errors in the determination of the material properties. The author has taken a part of the approach in reference (32) to formulate the model to identify the material parameters from a stress relaxation test. The basis of the fitting model is to evaluate the material response by analytical development of the constitutive equation and fit the experimental data by non linear regression analysis to determine the relaxation times (or viscosities). The development also takes care of the initially loading phase.

Stress relaxation test: In a classical stress relaxation test, a cylindrical glass specimen is subjected to an instantaneous strain and then the strain is held constant. Figure 4-11 shows an illustration of the cylinder compression test. Figure 4-12 shows the application of the strain and the decay of the stress. This is done at a suitable reference temperature. Owing to the viscoelastic nature of the material, the stress decays with constant strain due to the relaxation of the modulus. This decay of stress with time is noted from the experiment and fitted with the analytical results.

Analytical model: As discussed in the previous section the stress-strain relation for a viscoelastic material can be written as shown in Equation 4-22.

$$\underline{\sigma}(t) = K\varepsilon_v \underline{1} + \int_0^t G(t-s)\frac{d\underline{\varepsilon}(s)}{ds}ds \qquad 4\text{-}22$$

where, $G(t) = G_\infty + \sum_{i=1}^{N} G_i \exp(-t/\tau_i)$ is the relaxation function as discussed before, K is the bulk modulus, $\underline{1}$ is a unit vector and ε_v is the volumetric strain.

For the first part of the strain application i.e. strain for $t \in [0, t_t]$ from Figure 4-12(a) assuming linear strain, the strain function with time can be expressed by Equation 4-23

For $t \in [0, t_t]$

$$\underline{\varepsilon}(t) = \frac{\underline{\varepsilon}_1 t}{t_1}$$
$$\frac{d(\underline{\varepsilon})}{dt} = \frac{\underline{\varepsilon}_1}{t_1} \qquad 4\text{-}23$$

Hence for this part of the applied strain, the stress response is evaluated by evaluating analytically Equation 4-24 based on Equation 4-25.

$$\underline{\sigma}(t) = K\varepsilon_v \underline{1} + \frac{\varepsilon_1}{t_1}\int_0^t G(t-s)ds \qquad 4\text{-}25$$

Similarly for the latter part of the applied strain i.e. for $t \in (t_1, t_2]$ from 4-12(b) assuming constant strain, the strain function can be expressed by Equation 4-26

For $t \in (t_1, t_2]$

$$\underline{\varepsilon}(t) = \underline{\varepsilon}_1$$
$$\frac{d(\underline{\varepsilon})}{dt} = \underline{0} \qquad 4\text{-}26$$

The stress response for this part of constant strain is evaluated analytically by using Equation 4-26 in Equation 4-22. Equation 4-27 shows the stress response expression. The integral is broken into the separate time intervals.

$$\underline{\sigma}(t) = K\varepsilon_v \underline{1} + \int_0^{t_1} G(t-s)\frac{d\underline{\varepsilon}(s)}{ds}ds + \int_{t_1}^{t_2} G(t-s)\frac{d\underline{\varepsilon}(s)}{ds}ds \qquad 4\text{-}27$$

Hence Equation 4-27 and Equation 4-25 yield the analytical stress response which is fitted with the experimentally measured stress data by regression analysis. The regression is performed by minimizing the square sum of errors as shown by Equation 4-28

$$\min F = \sum_{i=1}^{N} \left(\sigma_i^{\text{experimental}} - \sigma_i^{\text{analytical}} \right)^2 \qquad 4\text{-}28$$

where F is the error function which is minimized and N is the number of sample points. As a result of the optimization routine as shown by Equation 4-28, we can determine the optimum values for the Maxwell parameters i.e. G_1, G_2, …, G_i, and $\eta_{1,}$ η_1, … , η_i. A part of this work has been published in (33).

However, the author was not able to implement this fitting routine because of unavailability of the test data from the cylindrical tests. There were limitations in the machine to perform this test and also obtaining cylindrical gobs was an issue because of its expense and availability.

Hence, for further implementations throughout this work, the author has assumed a single Maxwell element in the model and the viscosity of the glass provided by the manufacturer.

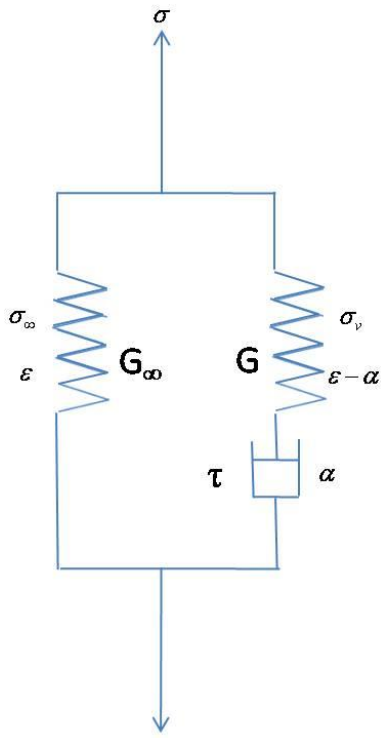

Figure 4-1. Standard linear model for viscoelasticity

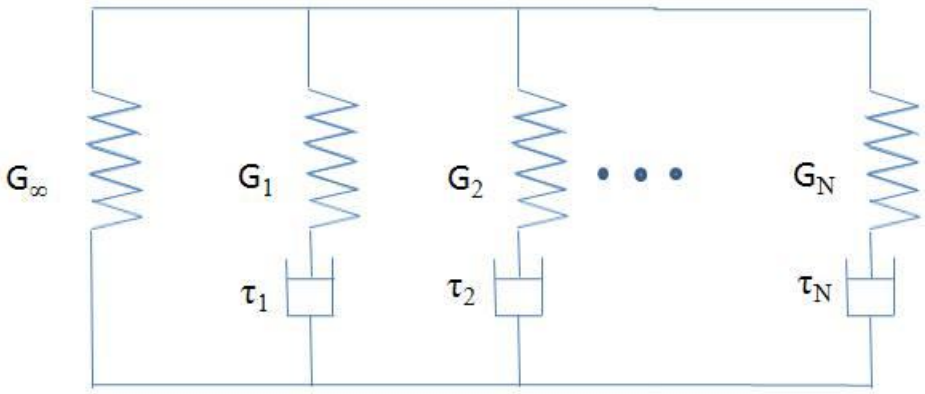

Figure 4-2. Generalized Maxwell model for viscoelasticity

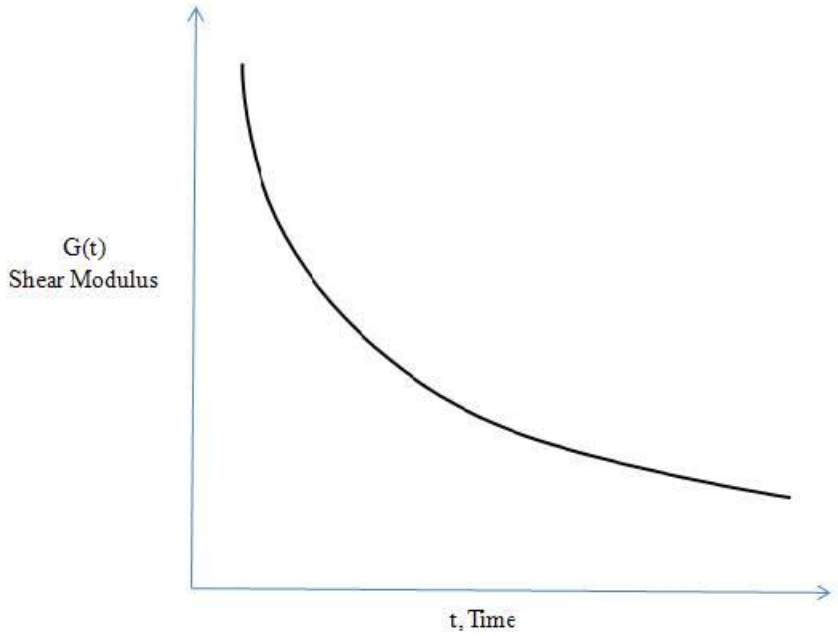

Figure 4-3. Exponential decay of modulus for a viscoelastic material

A 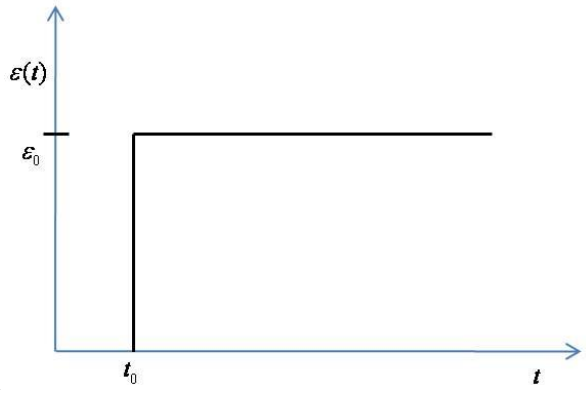

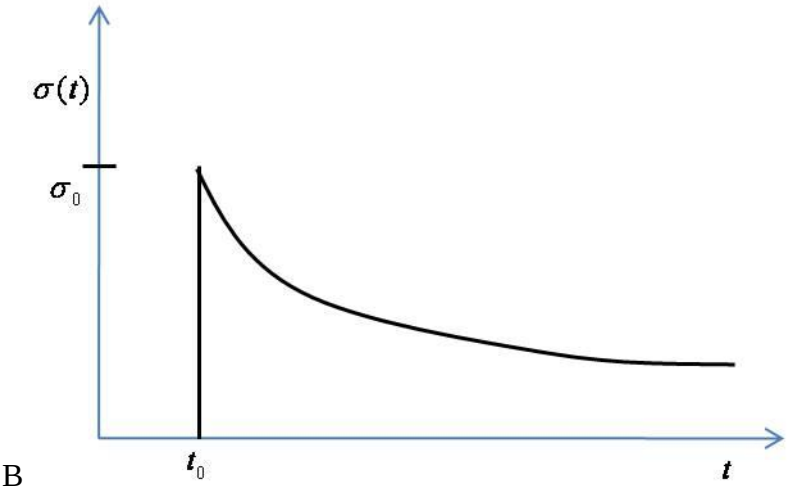

B

Figure 4-4. Stress response of a viscoelastic material. A) Material subjected to an instantaneous strain and then held constant. B) The corresponding stress response, which decays over time though the strain is constant.

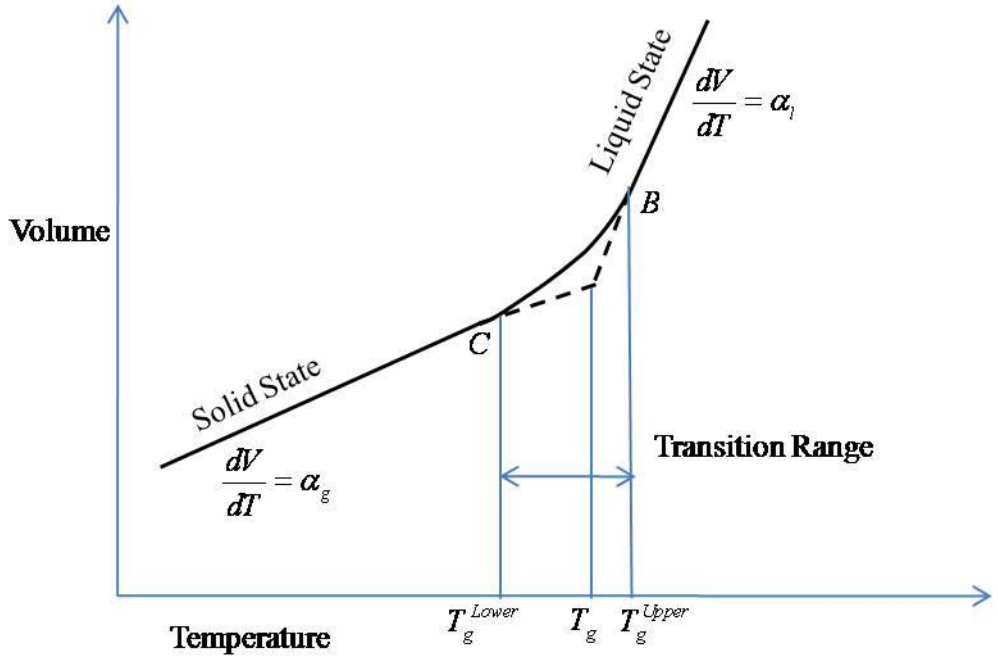

Figure 4-5. Volume vs. temperature behavior for a viscoelastic material like glass.

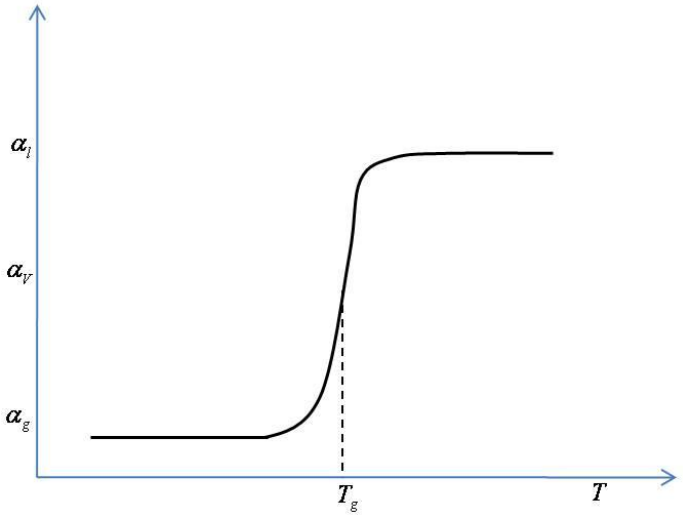

Figure 4-6. Behavior of a property like coefficient of thermal expansion with temperature for a viscoelastic material like glass.

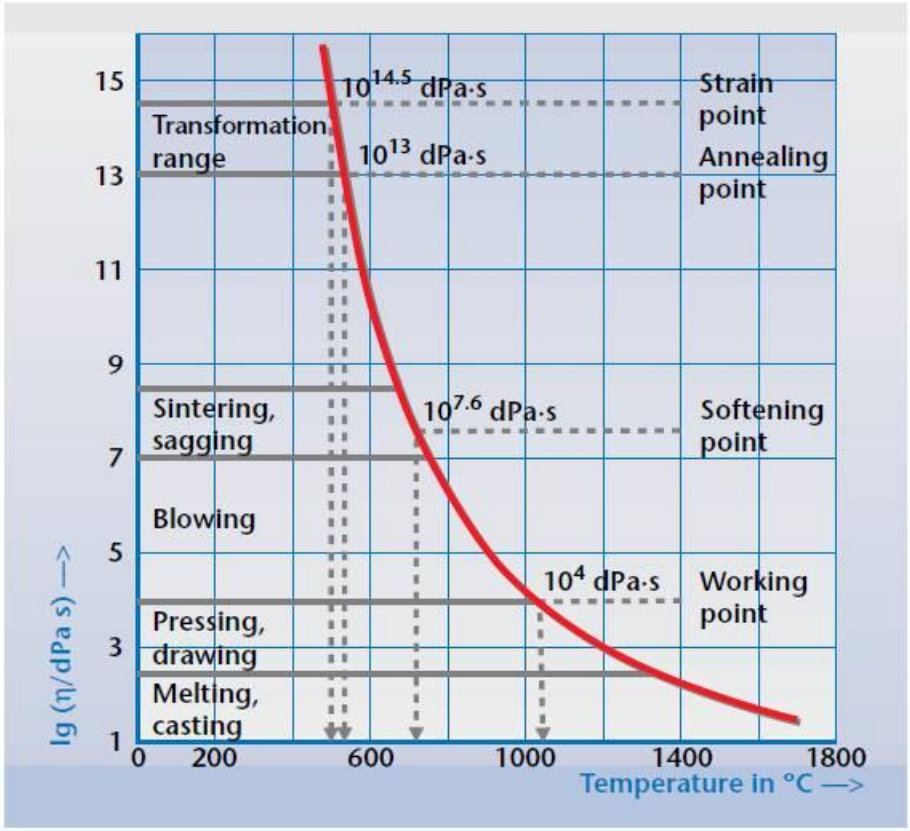

Figure 4-7. Temperature vs. viscosity graph for a typical glass

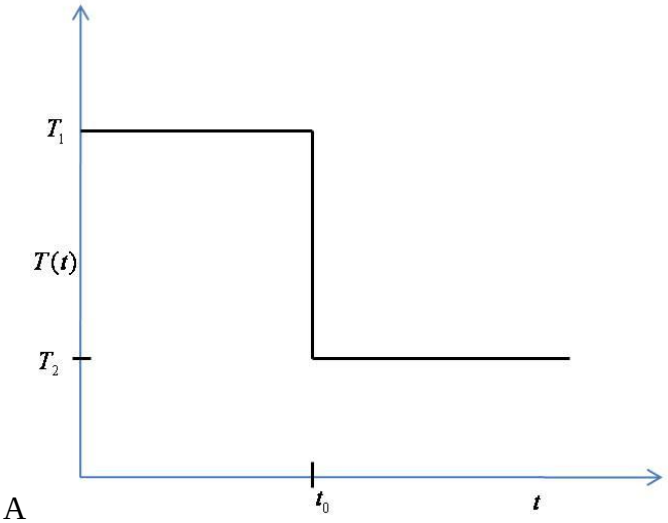

A

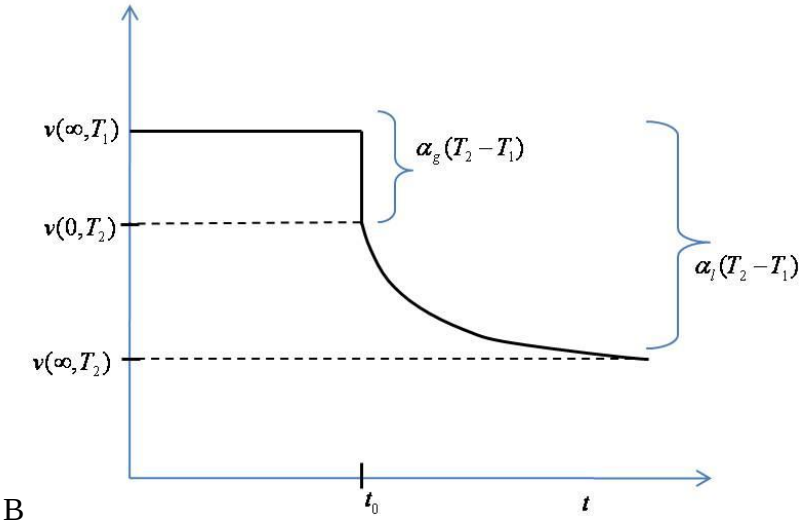

B

Figure 4-8. Phenomenon of structural relaxation A) Viscoelastic material subjected to a step change in temperature B) Corresponding response of a property like volume for e.g. with time when subjected to a step change in temperature

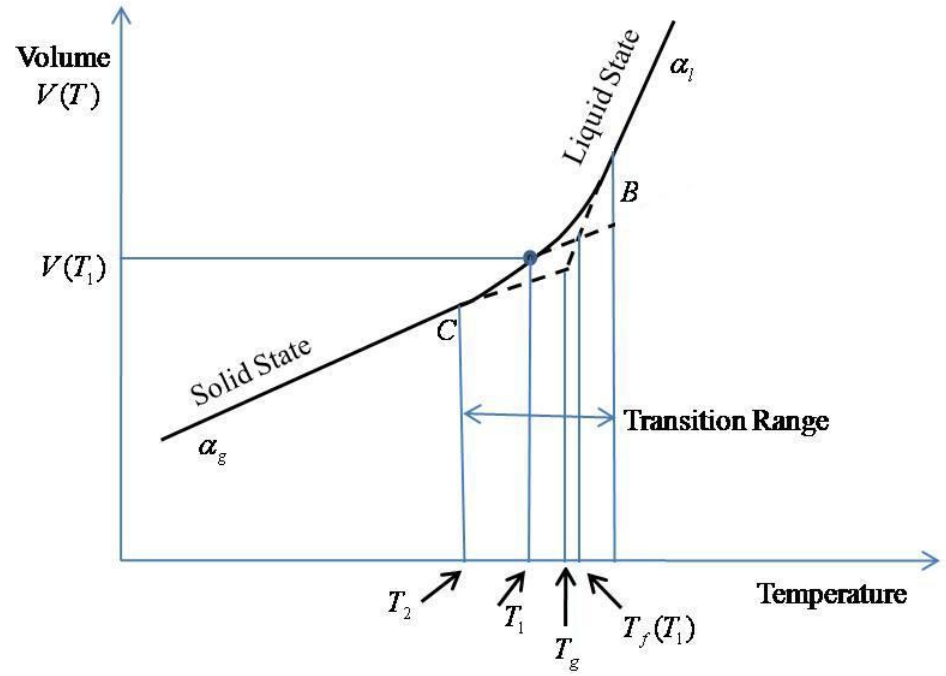

Figure 4-9. Calculation of fictive temperature in the transition range

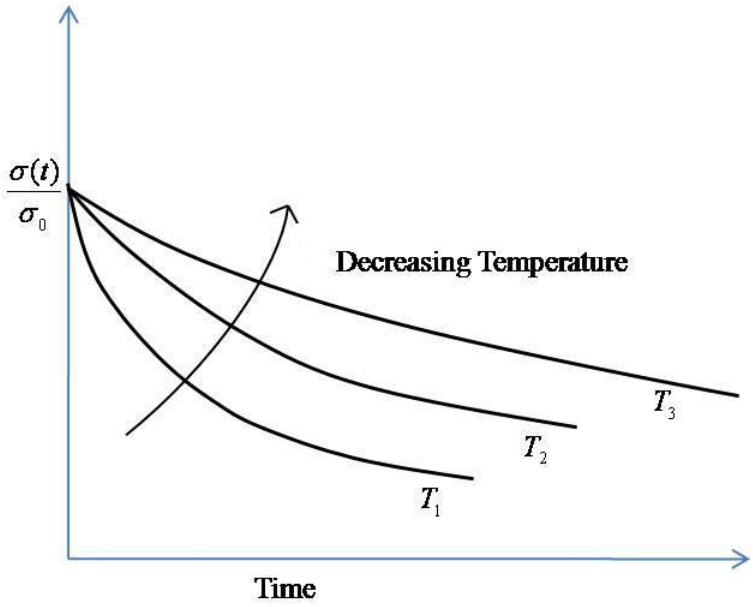

Figure 4-10. Variation of relaxation curves of a viscoelastic material with decreasing temperature

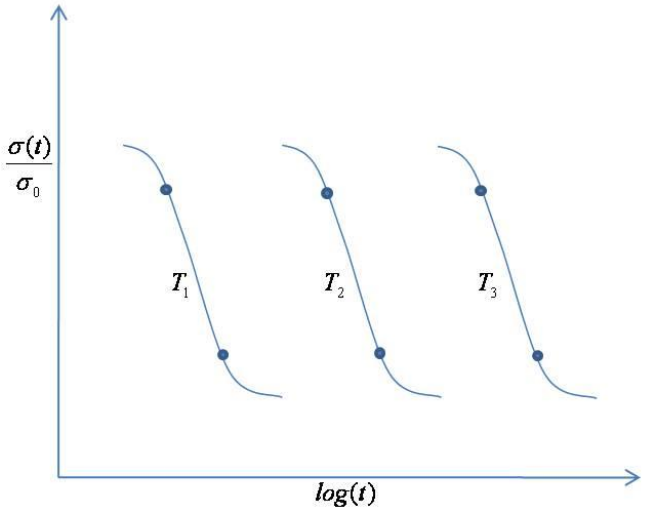

Figure 4-11. Relaxation curves at different temperatures plotted on a log(time) scale.

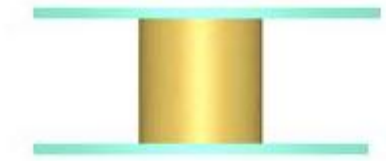

Figure 4-12. Classical cylinder compression test (ABAQUS)

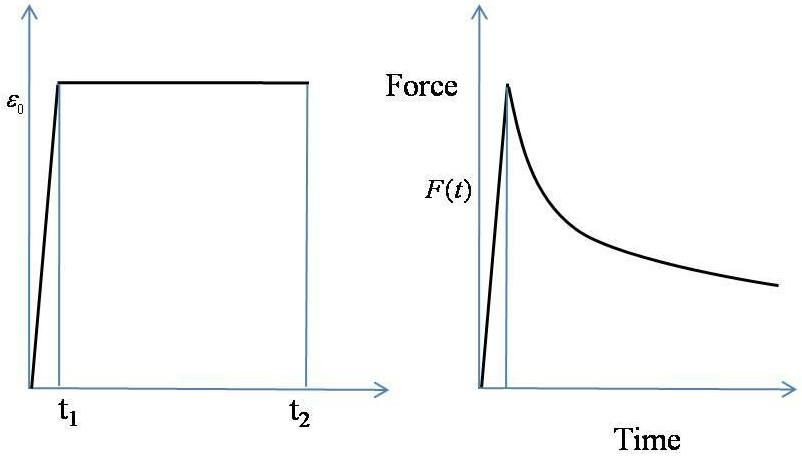

Figure 4-13. Application of strain function and force decay for a cylinder compression test

CHAPTER 5
MNTS GLASS MOLDING PROCESS

A custom designed glass molding machine, GPM 065-S, was developed at Moore Nanotechnology Systems (MNTS) based in Keene, NH for the glass molding research. The 065-S represents the fact that the machine molding chamber can accommodate to a maximum of 65 mm and is a single molding chamber machine. The numerical prediction of the glass molding process was simulated according to the molding process designed on GPM 065-S. The main process controller is a PC based controller that utilizes PID feedback and has software PLC's.

Figure 5-1 shows the molding machine. The glass molding process is essentially performed in five cycles which can be programmed into the machine using HMI (Human Machine Interface). The five cycles involved in the glass molding process are:

1. Heating Cycle
2. Soaking Cycle
3. Pressing Cycle
4. Gradual Cooling Cycle
5. Rapid Cooling Cycle

A typical glass press molding cycle is composed from the above five cycles sequentially; heating the glass and mold, soaking the glass to achieve uniform temperature, pressing the glass to obtain the deformed lens shape, gradually cool the lens to ensure uniform cooling and finally rapid cooling to room temperature. Figure 5-2 shows the five cycles of the glass pressing molding. Each cycle is described briefly in the following sections and the numerical simulation of the cycles is discussed in the next chapter.

Heating Cycle

The heating is the first step in glass press molding. Before the heating process starts the system is purged with Nitrogen to remove any oxygen from the environment. Nitrogen purge is set in seconds. At the end of the purge cycle the heating cycle commences. Two temperature

probes at the top and the bottom of the mold monitor the temperature. The thermocouples are used to sense the temperature and feedback into the PID loop for control. The heating effect is obtained through infra red heating using infra red lamps. Figure 5-3 illustrates the heating of the mold chamber with the glass gob inside. The infrared lamps are embedded inside a water cooled chamber as shown in Figure 5-4 (the solid model figure). The present machine has a capability to achieve a maximum of 800 ºC with a precision of about 1 ºC.

The heating process will bring the molds up to the commanded temperature by the closed loop control between the thermocouples and the lamps. Usually the molds do not undergo any compression during this cycle. Any compression will most likely destroy the glass sample. Typically, the commanded temperature is slightly above the glass transition temperature where the glass is soft enough for pressing. Typical values range from 5-10% above T_g. The molds and the glass sample expand during this cycle due to the thermal effects.

Soaking Cycle

The soaking cycle is necessary for the temperature of the glass and the molds to reach a steady state, where all the components are at a uniform temperature distribution. The controller maintains the commanded temperature during of the soaking cycle time. On large size molds and glass samples the soaking time can be on the order of few minutes to ensure that the temperature is uniform. During this cycle the controller is still operating under position control.

Pressing Cycle

The pressing cycle commences at the end of the soaking cycle. During this cycle the controller maintains the commanded temperature and will start moving the pressing axis to compress the glass sample. In the cycle, the controller can be either operated in position or force control. If operating in position control, the user must ensure that the expansion of the molds and glass material will not create excessive forces on the molds and glass. Since molds are highly

rigid, even a slight inaccuracy in specifying the displacement or position can result in very high reaction forces. Hence the pressing process is generally performed under the force control mode where the amount of force to be applied is specified. Under force control mode, the expansion compensation is not necessary because the press will automatically move to maintain the commanded force. The molding area is enclosed with metal bellows to enable molding in a vacuum or inert gas environment. This will help to prevent oxidation damage to the mold surfaces at the elevated temperatures, and will help to prevent dust and other contaminants from collecting on the mold surfaces. The fully enclosed molding chamber with vacuum will help to minimize the convective and radiation heat losses.

The pressing cycle is initiated by an electro-mechanical actuator and a load cell is used for the force sensing. The maximum pressure that can is applied is about 13000 N. Position is sensed using an encoder on the servomotor that drives the electro-mechanical actuator.

Gradual Cooling Cycle

The gradual cooling is the fourth step in the glass press molding process. In this step the temperature of the molds and glass is gradually decreased to a desired temperature. Usually additional heat is required to ensure that the molds do not cool too fast. The gradual cooling is done by continuously injecting heat and Nitrogen gas to follow the specified temperature profile. During this phase it is possible to press again to give the glass a final shape and alignment. The temperature and force variation is shown in Figure 5-5.

This cycle is the most critical cycle in the glass molding process. During the cooling, the outer surface of the glass cools faster than the inner surface which results in a non-uniform temperature distribution. During the temperature range where the phase changes, the outer surface approaches the elastic state while the inner core is still viscous. This non-uniform temperature distribution and the phase change results in residual stresses, which are detrimental

to the performance of the optical element. Hence, the cooling has to be carefully controlled to minimize the non-uniform temperature distribution. This allows enough time for the stresses to relax and attain equilibrium with every step change in temperature.

Rapid Cooling Cycle

Rapid cooling is the last cycle in the process and it takes the molds and glass temperature to ambient temperature. The cooling is accomplished using a high flow of nitrogen gas. After this cycle is completed the glass in unloaded from the molds and a new glass gob is loaded. The rapid cooling generally is started from the lower range of the glass transition range where the glass can be considered to be frozen into a solid.

Figure 5-1. A custom designed molding machine (GPM065-S) developed at MNTS.

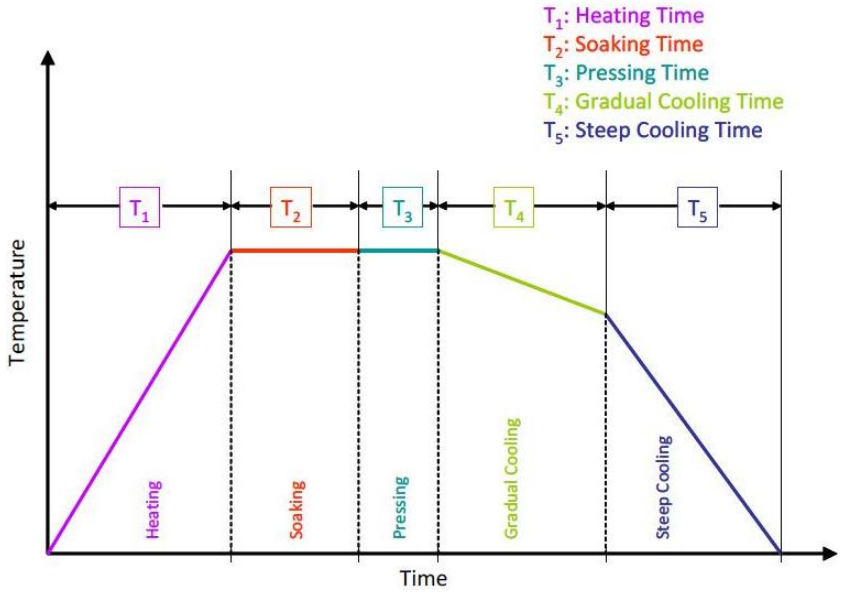

Figure 5-2. Different cycles in a typical glass molding process

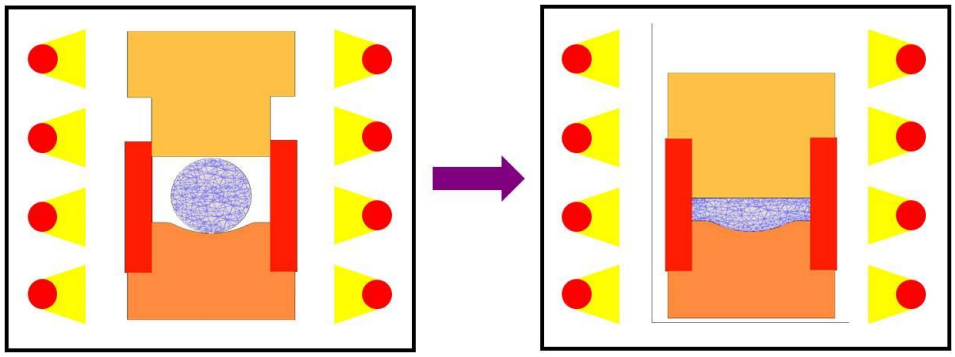

A

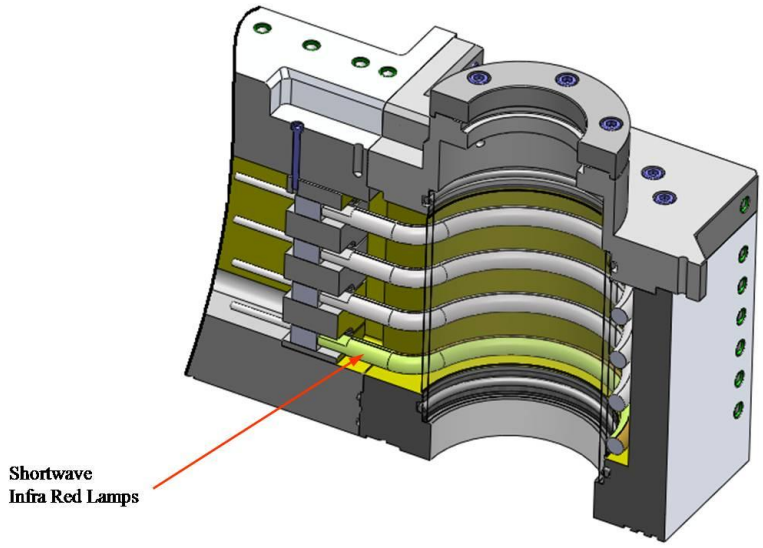

B

Figure 5-3. Infrared heating in the heating cycle. A) schematic of the heating process. B) The solid model of the actual glass molding chamber

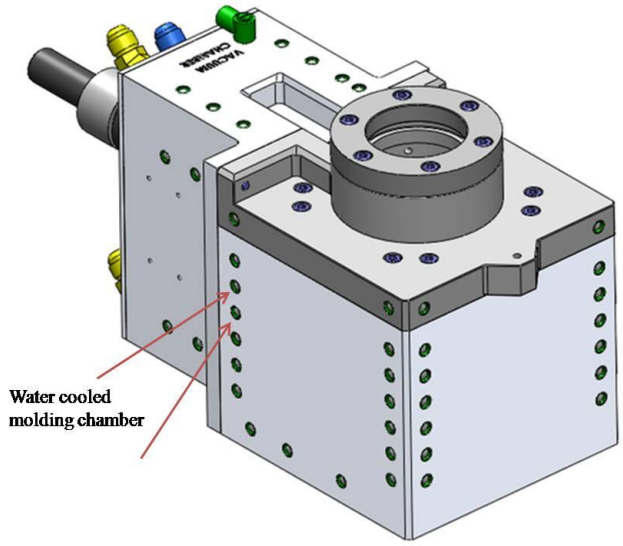

Figure 5-4. Solid model of the glass molding chamber

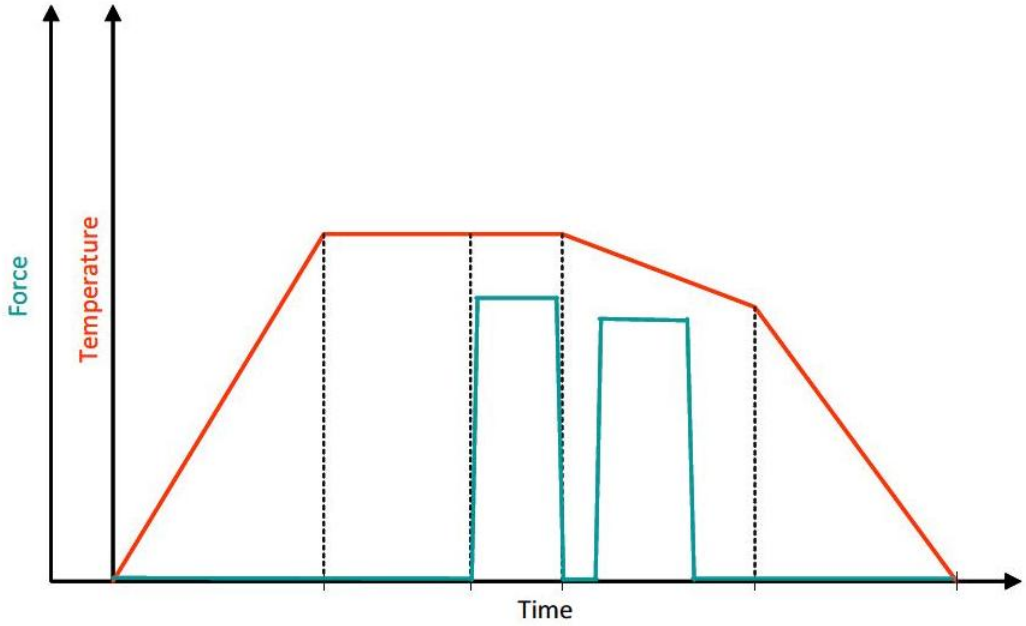

Figure 5-5. The temperature force variation in a glass molding process

CHAPTER 6
NUMERICAL SIMULATION OF GLASS MOLDING PROCESS USING THE FINITE ELEMENT METHOD

Numerical Model of the Glass Molding Process

This chapter discusses the numerical simulation of the glass molding process as described in Chapter 5 using the finite element method. Here, in this preliminary approach, each cycle has been discreetly analyzed and the important phenomena affecting the molding process have been quantified. The discreet cycle-by-cycle analysis is a more engineering oriented approach to model the glass molding process which would make the numerical tool computationally efficient, monetarily affordable and yet good enough for manufacturing purposes. Although commercially available software have the capability to simulate the process, but none of them are customized fully for the simulation of glass molding process. They would be more of a brute force approach to the problem. This is the first attempt to develop a highly customized tool for predicting the glass molding process and would be used with the MNTS GPM machine to aid the users to predict the process without having to perform the molding process. This would eradicate the need for iteratively perform the molding process and obtain the optimal design of the molding process to result in the desired optical product. The simulation of each cycle is described in the following sections.

The finite element simulation was coded in Intel FORTRAN 10 and C# was used for the pre processing and the post processing of the results. Four node quadrilateral elements have been used all throughout the simulation. Because of rotational symmetry of most of the optical devices, the entire simulation was modeled as an axisymmetric formulation for computational simplicity.

Heating Cycle

Objectives

During the heating phase of the glass and the molds to the molding temperature, the profile of the glass and most importantly the molds change due to thermal expansion. It is important to quantify the change in mold profile so as to obtain the accurate pressing surface for the molding. Linear thermal analysis was performed for the heating cycle on the glass and the molds using the finite element method. The objective at the end of this cycle was to capture the thermal expansion of the mold profile and the expansion of glass.

Assumptions and Limitations

1. The molds and the glass are assumed to be elastic bodies during this cycle as the Tungsten Carbine (WC) molds are really stiff, rigid and inert. Hence it is a reasonable assumption to consider them as perfectly elastic bodies.
2. Because of the fact that at the end of the heating cycle, a soaking cycle is performed, no dynamic effects were taken into consideration. At the end of this process, the molds and the glass were assumed to have achieved a steady state of uniform temperature due to the soaking cycle.

Theory and Implementation

Elastic thermal analysis: The constitutive equation governing the stress-strain relations for an elastic thermal analysis can be given by Equation 6-1

$$\underline{\sigma} = \underline{D}(\underline{\varepsilon} - \underline{\varepsilon}^{th}) \qquad 6\text{-}1$$

where, σ[1] is the stress tensor, ε is the actual strain tensor, ε^{th} is the thermal strain vector which is given by $\alpha\Delta T$ for elastic analysis with α being the coefficient of thermal expansion and ΔT being the change in temperature, and D is the elastic modulus matrix. For finite element implementation the stress-strain relations are converted to equations relating forces on nodes to

[1] Underlined quantities in the equations are to be considered as tensors (or vectors) as applicable

nodal displacements. The strain field can be expressed by the interpolating functions by Equation 6-2.

$$\underline{\varepsilon} = \underline{B}\underline{u} \qquad 6\text{-}2$$

where B is the derivative of the finite element shape function matrix of a four node quadrilateral element and u is the displacement vector. Similarly the thermal load vector can be constructed in terms of forces on nodes as give in Equation 6-3.

$$\underline{F}^{th} = \int_{\Omega} \underline{B}^{T} \underline{D}\underline{\varepsilon}^{th} d\Omega \qquad 6\text{-}3$$

where B^T is the transpose of B matrix and Ω is domain of integration.

By multiplying Equation 6-1 with B^T and use Equation 6-2 and Equation 6-3 we have Equation 6-4

$$\underline{F}^{ext} = \int_{\Omega} \underline{B}^{T} \underline{\sigma} d\Omega = \int_{\Omega} \underline{B}^{T} \underline{D}\underline{B}\underline{u} d\Omega - \underline{F}^{th} \qquad 6\text{-}4$$

where, F^{ext} is the applied external force. Since there is no externally applied mechanical load, the LHS of Equation 6-4 vanishes. Writing Equation 6-4 in finite element form we have Equation 6-5 which is solved for obtaining nodal displacements.

$$[K]\{u\} = \{F\} \qquad 6\text{-}5$$

where, $K = \int_{\Omega} \underline{B}^{T} \underline{D}\underline{B} d\Omega$ is the global stiffness matrix and $F = F^{th} = \alpha \Delta T$ is the thermal load vector and u is the vector of nodal displacements. Here ΔT is the difference between the room temperature and the molding temperature. Hence $\Delta T = T_{molding} - T_{room}$

Once Equation 6-5 is solved for nodal displacements, the new thermally expanded profile of the mold is extracted by adding the nodal displacements to the original mold surface profile as given by Equation 6-6.

$$(\underline{P}_{new}) = (\underline{d}_{thermal}) + (\underline{P}_{old}) \qquad 6\text{-}6$$

where ($\underline{P}_{new}$) is the new profile of the mold surface, ($\underline{d}_{thermal}$) is the vector of displacements from the thermal analysis, and ($\underline{P}_{old}$) is the initial profile of the mold. The thermally expanded profile is used for the pressing analysis which is discussed in the next section.

Pressing Cycle

Objectives

During the pressing process, when the molding temperature has been achieved after the heating cycle, the upper mold is pressed over the soft glass to mold the glass into the desired imprint of the lower and upper molds. The pressing process is performed with the temperature being held constant, i.e. the pressing process is essentially isothermal. The objective of this cycle is to obtain the shape of glass at the end of the pressing cycle.

Assumptions and Limitations

1. Since glass is soft at the molding temperature and the molds are highly stiff and rigid, the mold surfaces are assumed to be rigid surfaces.
2. Since the pressing takes place in an isolated vacuum chamber, we assume the pressing cycle to be completely isothermal
3. Since glass is nearly an incompressible fluid at higher temperatures, we have considered relaxation only in the shear component and have assumed the bulk component to be constant throughout the cycle.
4. The friction data between the mold coating and the glass could not be obtained. But, because of the presence of the coating which reduced the friction by a great factor and eradicates sticking, the friction between the molds and the glass was considered negligible.

Theory and Implementation

Constitutive equation: We discussed the constitutive stress-strain relation for a one dimensional formulation in Chapter 4. The three dimensional form of the constitutive relation can be expressed by Equation 6-7. As we have assumed the relaxation to occur only in the stress deviator, the constitutive equation is expressed by the split of the deviatoric and the bulk components.

$$\sigma = \int_0^t 2G(t-s)\frac{d\underline{e}}{ds}ds + K\varepsilon_v \underline{1} \qquad 6\text{-}7$$

where, e is the deviatoric strain vector, K is the bulk modulus, **1** is the unit tensor and ε_v is the volumetric strain. We can see that the shear component is viscoelastic and the bulk component has been formulated according to elastic relations. G(t-s) is the shear relaxation kernel function as discussed in Chapter 4 and is described by Equation 6-8.

$$G(t) = G_0\left(w_\infty + \sum_{i=1}^{N} w_i \exp(-t/\tau_i)\right) \qquad 6\text{-}8$$

where, G_0 is the modulus at t=0 i.e. $G_0 = G_\infty + \sum_{i=1}^{N} G_i$, 'i' is the i^{th} Maxwell element, N is the total number of Maxwell elements and w_∞ and w_i are the normalized weights defined as $w_\infty = \frac{G_\infty}{G_0}$ and $w_i = \frac{G_i}{G_0}$ such that $w_\infty + \sum w_i = 1$

Numerical Integration: For performing the finite element analysis, the integral equation in Equation 6-7 needs to be integrated. The integration scheme proposed by Simo (34)and Taylor (35) is adapted. Here only the deviatoric component integration is outlined as the bulk component is elastic. Hence, the deviatoric stress given by Equation 6-7 using Equation 6-8 can be given by Equation 6-9.

$$\underline{s} = 2G_0\int_0^t \left(w_\infty + \sum_{i=1}^{N} w_i \exp\left(\frac{-t+s}{\tau_i}\right)\right)\frac{d\underline{e}}{ds}ds \qquad 6\text{-}9$$

Breaking the stress response expressed in Equation 6-9 into components we have Equation 6-10

$$\underline{s} = \underline{s}_\infty + \sum_{i=1}^{N} \underline{s}_i \qquad 6\text{-}10$$

$$= 2G_0 \int_0^t w_\infty \frac{d\underline{e}}{ds} ds + 2G_0 \int_0^t \sum_{i=1}^{N} w_i \exp\left(\frac{-t+s}{\tau_i}\right) \frac{d\underline{e}}{ds} ds \qquad 6\text{-}10$$

For the Newton-Raphson solution procedure for the finite element analysis we develop a recursive stress update for Equation 6-10. Assuming that deviatoric stress is known at load step 'n', we calculate the stress update for step 'n+1'. The first stress component of Equation 6-10 can be expressed as in Equation 6-11

$$s_\infty^{n+1} = 2Ge_\infty^{n+1} \qquad 6\text{-}11$$

For simplicity, we consider the i[th] Maxwell element for the evaluation of the second stress component of Equation 6-10. At 'n+1' we have the stress component given by Equation 6-12

$$\underline{s}_i^{n+1} = 2G_i \int_0^{t_{n+1}} \exp\left(\frac{-t_{n+1}+s}{\tau_i}\right) \frac{d\underline{e}}{ds} ds \qquad 6\text{-}12$$

$$= 2G_i \int_0^{t_n} \exp\left(\frac{-t_n - \Delta t + s}{\tau_i}\right) \frac{d\underline{e}}{ds} ds + 2G_i \int_{t_n}^{t_{n+1}} \exp\left(\frac{-t_{n+1}+s}{\tau_i}\right) \frac{d\underline{e}}{ds} ds \qquad 6\text{-}12$$

The first term of Equation 6-12 can be expressed as $s_i^n \exp\left(\frac{-\Delta t}{\tau_i}\right)$ in terms of the stress during the previous load step. Using the midpoint rule for time integration for the second term, Equation 6-12 can be expressed as shown in Equation 6-13 (36)

$$\underline{s}_i^{n+1} = \exp\left(\frac{-\Delta t}{\tau_i}\right) \underline{s}_i^n + 2G_i \exp\left(\frac{-\Delta t}{2\tau_i}\right) \Delta\underline{e} \qquad 6\text{-}13$$

where $\Delta e = e_{n+1} - e_n$.

Hence the total stress using the stress terms given by Equation 6-14, Equation 6-12 and Equation 6-7 can be expressed as shown in Equation 6-15.

$$\underline{\sigma}^{n+1} = p^{n+1} + \underline{s}_\infty^{n+1} + \sum_{i=1}^{N} \underline{s}_i^{n+1} \qquad 6\text{-}15$$

where $p^{n+1} = K\varepsilon_v \underline{1}$ is the bulk response.

Large deformation viscoelasticity: Since the nature of deformation in the glass molding process is large, the stresses are formulated in terms of rotated stresses to account for the rotation (37). The rotated deviatoric component of stress is expressed as $\underline{\Sigma} = \underline{R}^T \underline{s}\underline{R}$ where R is the rotation arising from the polar decomposition of the deformation gradient F. Hence, rotated stress is expressed as shown in Equation 6-15, which is analogous to Equation 6-9

$$\Sigma = 2\int_0^t G_\infty \left(\underline{R}^T \underline{d}\underline{R}\right) ds + 2\int_0^t \sum_{i=1}^{N} G_i \exp\left(\frac{-t+s}{\tau_i}\right)\left(\underline{R}^T \underline{d}\underline{R}\right) ds \qquad 6\text{-}15$$

where d is the deviatoric part of the rate of deformation tensor $\underline{D} = \frac{1}{2}\left(\frac{\partial \Delta u}{\partial x} + \frac{\partial \Delta u^T}{\partial x}\right)$. In finite element implementations, the rate of deformation tensor is replaced by the strain increment as given by Equation 6-16.

$$D_{n+\frac{1}{2}} \Delta t \approx \Delta\varepsilon_{n+\frac{1}{2}} = \frac{1}{2}\left(\frac{\partial \Delta u}{\partial x} + \frac{\partial \Delta u^T}{\partial x}\right) \qquad 6\text{-}16$$

Using Equation 6-16, Equation 6-15 and the fact that $\underline{\Sigma} = \underline{R}^T \underline{s}\underline{R}$, the deviatoric stress component for i[th] Maxwell element in terms of rotated stresses can be expressed by Equation 6-17

$$s_i^{n+1} = \exp\left(\frac{-\Delta t}{\tau_i}\right)\Delta R(s_i^n)\Delta R^T + 2G_i \exp\left(\frac{-\Delta t}{2\tau_i}\right)\Delta R_{n+\frac{1}{2}}(\Delta e_{n+\frac{1}{2}})\Delta R^T_{n+\frac{1}{2}} \qquad 6\text{-}17$$

where, $R_{n+1,} R_{n+\frac{1}{2}}, R_n$ are the rotation tensors arising from the polar decomposition of the deformation gradients $F_{n+1,} F_{n+\frac{1}{2}}, F_n$ respectively and $\Delta R = R_{n+1} R_n^T$, $\Delta R_{\frac{1}{2}} = R_{n+1} R^T_{n+\frac{1}{2}}$, $\Delta e_{n+\frac{1}{2}}$ is the deviatoric component of $\Delta\varepsilon_{n+\frac{1}{2}}$.

The total Cauchy stress expression was given in Equation 6-14. Considering the rotational effects the same equation can be expressed as in Equation 6-18

$$\sigma^{n+1} = p^{n+1} + s_{\infty}^{n+1} + \sum_{i=1}^{N} s_i^{n+1} \qquad 6\text{-}18$$

where $p^{n+1} = p^n + K\varepsilon_v^{n+1}\underline{1}$, $s_{\infty}^{n+1} = \Delta R(s_{\infty}^{n+1})\Delta R^T + 2G_{\infty}\Delta R_{\frac{1}{2}}(\Delta e_{1/2})\Delta R_{\frac{1}{2}}^T$ and s_i as in Equation 6-17.

The nonlinear finite element equations arising from the stress equation as defined in Equation 6-18 are solved by Newton-Raphson iterative method. The iterations are performed until the force residual is zero.

Cooling Cycle

Objectives

During the cooling or annealing of the formed glass lens from the pressing temperature to the room temperature it is important to make sure that the residual stresses that result are minimum due to the non uniform cooling and phase change of glass from the pressing temperature to the room temperature. The presence of residual stresses leads to an inhomogeneous refractive index which will deteriorate the optical performance of the lens.

Hence the objective of this cycle is to capture the residual stresses that arise during the cooling of the glass and also estimate the shrinkage of the glass that would give the final profile of the glass at the end of the molding process. As a consequence we will also be able to predict the temperature distribution during the rapid and at the end of the gradual cooling phases.

Assumptions and limitations

1. At the end of the pressing process, because of the very small relaxation times it is assumed that the glass sample is completely deviatoric stress free at the start of the cooling process.
2. Because of the isothermal process, the initial temperature conditions for the glass can be considered as a uniform temperature distribution i.e. the pressing temperature.

3. Since majority of the heat from the glass is lost to the molds, and the mold surfaces are almost in contact with the glass, the outer periphery of the glass is assumed to have the same temperature as that of the mold. Hence, the temperature reported by the thermocouple is assumed to be the boundary condition for the glass nodes on the periphery.

Theory and implementation:

Transient thermal analysis: Since the cooling of glass is a time dependent heat transfer problem, a transient thermal analysis is required to obtain the temperature distribution at the end of the gradual and rapid cooling cycles. The governing equation of interest for the transient first order cooling can be written as shown in Equation 6-19.

$$[C]\{\dot{T}\}+[K]\{T\}=\{F^a\} \qquad 6\text{-}19$$

where, [C] is the thermal damping matrix, [K] is the thermal conductivity matrix, {T} is the vector of nodal temperatures, $\{\dot{T}\}$ is the time rate of nodal temperature change and $\{F^a\}$ is the applied thermal load vector.

The procedure employed for the finite element solution of Equation 6-19 is the generalized trapezoidal rule (38). Hence the temperature at time step 'n+1' can be written by Equation 6-20

$$\{T_{n+1}\}=\{T_n\}+(1-\theta)\Delta t\{\dot{T}_n\}+\theta\Delta t\{\dot{T}_{n+1}\} \qquad 6\text{-}20$$

where, θ is the transient time integration parameter, subscripts 'n' and 'n+1' represent quantities at the respective time steps and $\Delta t=t_{n+1}-t_n$.

Equation 6-19 at time t_{n+1} can be written as shown in Equation 6-21

$$[C]\{\dot{T}_{n+1}\}+[K]\{T_{n+1}\}=\{F^a\} \qquad 6\text{-}21$$

Now, by substituting $\{\dot{T}_{n+1}\}$ from Equation 6-20 leads us to Equation 6-22.

$$\left(\frac{1}{\theta\Delta t}[C]+[K]\right)\{T_{n+1}\}=\{F^a\}+[C]\left(\frac{1}{\theta\Delta t}[T_n]+\frac{1-\theta}{\theta}\{\dot{T}_n\}\right) \qquad 6\text{-}22$$

The above Equation 6-22 is used for solution of temperature in the finite element analysis. The initial condition at the start of the analysis is provided as a uniform temperature field which is the pressing temperature. For the finite element analysis, the quantities in Equation 6-22 are defined by the Equations 6-23.

$$\begin{aligned} [C] &= \rho c \int_{\Omega} \{N^T\}\{N\}\, d\Omega \\ [K] &= \int_{\Omega} \{B^T\}[k]\{B\}\, d\Omega \\ F^a &= \underline{0} \end{aligned} \qquad \text{6-23}$$

where, N is the vector of element shape functions, B is matrix of the derivative of the shape functions, ρ is the density of glass, c is the specific heat of glass and [k] is the thermal conductivity matrix. F^a which is the external thermal load vector is set to zero as there are no externally applied thermal loads.

A value of 1 is used for the transient time integration parameter, which is also known as the backward Euler method. For this value the solution of these equations are unconditionally stable, i.e., stability is not a factor of the time step Δt selection. However, smaller values of Δt are recommended for accurate results.

This temperature distribution that results for the transient thermal analysis will be used to obtain the free thermal strain which will be used further to calculate the residual stresses.

Structural relaxation time: Structural relaxation refers to the time dependent response of a property like volume to change in temperature. The structural response of glass to a step change in temperature is inherently non-linear and depends on the magnitude and direction of step change. The non-linearity occurs because the changing structure alters the viscosity and hence the rate of relaxation.

As discussed in Chapter 4, the glass transition is a region of temperature in amorphous materials like glass where molecular rearrangements occur on a scale of minutes or hours

because of which the property change of the liquid is easily observed. At temperatures well above the glass transition temperature, equilibrium structure is attained almost instantaneously as glass is in a liquid state and at temperatures lower to the glass transition temperature; glass is highly viscous and exists as a solid.

The change of a property like volume against temperature change is shown in Figure 4-5 in Chapter 4. As discussed in Chapter 4, the fictive temperature can be calculated using the Boltzmann superposition principle for an arbitrary thermal history by Equation 4-21, which is reproduced in Equation 6-24 here for convenience.

$$T_f(t) = T(t) - \int_0^t M_v(t-s)\frac{dT(s)}{ds}ds \qquad 6\text{-}24$$

Where M_v is the structural response function given by Equation 4-17 in Chapter 4.

However, for calculation of fictive temperatures in the finite element implementation, the algorithm proposed by Markovsky and Soules has been adopted as outlined in reference (39). The authors showed that the routine is efficient and stable. The authors expressed the response function as a sum of exponential relaxations and used the differential form of Equation 6-24. Initial values of the partial fictive temperatures are assigned and numerically integrated in the transient thermal analysis. The update formula for the fictive temperature calculation is given by Equation 6-25 with $T_f(0) = T_0$

$$T_f(t) = \frac{T_f(t-\Delta t) + T(t)(\Delta t/\tau)}{1+\Delta t/\tau} \qquad 6\text{-}25$$

Calculation of free thermal strain: Once the fictive temperature is calculated using the methods stated in previous section, the thermal strain including the effects of structural relaxation can be calculated. For a temperature change of $\Delta T=T_1-T_2$ as shown in Figure 4-9 in Chapter 4, the thermal strain can be expressed as given in Equation 6-26.

$$\Delta\varepsilon^{th} = \alpha_g \Delta T + \left(\alpha_l - \alpha_g\right)\Delta T_f \qquad 6\text{-}26$$

where, α_g is the coefficient of thermal expansion in solid state, α_l is the coefficient of thermal expansion in the liquid state and ΔT_f is the change in the fictive temperature.

We can see from Equation 6-27 that initially, when glass is in a liquid state, the relaxation time τ is very close to zero hence the fictive temperature is initially equal to 0. Hence Equation 6-26 reduces to $\Delta\varepsilon^{th} = \alpha_l \Delta T$. Gradually the fictive temperature increases and when glass approaches the state of elasticity, where the relaxation time is really high, the fictive temperature achieves a constant value which is the glass transition temperature as evident from Equation 6-26. The thermal strain during that state becomes $\Delta\varepsilon^{th} = \alpha_g \Delta T$ which is elastic thermal strain. Between these two phases, at the glass transition temperature, the thermal strain is given by Equation 6-26.

Calculation of residual stress

Thermoelasticity: For a thermoelastic analysis, the stress strain relation is given by Equation 6-27.

$$\underline{\sigma} = \underline{C}\left(\underline{\varepsilon} - \underline{\varepsilon}^{th}\right) \qquad 6\text{-}27$$

where, $\underline{C} = K\left(\underline{1}\otimes\underline{1}\right) + 2G\underline{I}_{dev}$ is the constitutive matrix for an elastic material with $\underline{1}$ being a second-order unit tensor, and $\underline{I}_{dev}$ being the deviatoric part of an identity tensor, ε is the mechanical strain and ε^{th} is the thermal strain. For the finite element implementation, the stress-strain equations are converted to equations representing nodal forces and nodal displacements. The strain ε for the finite element formulation can be expressed in terms of nodal displacements by Equation 6-28.

$$\underline{\varepsilon} = \underline{B}\underline{u} \qquad 6\text{-}28$$

where, B matrix is the derivate of the finite element shape functions and u is the vector of nodal displacements. The thermal load vector can be constructed as given in Equation 6-29

$$\underline{F}^{th} = \int_{\Omega} \underline{B}^{T} \underline{\sigma} d\Omega = \int_{\Omega} \underline{B}^{T} \underline{C} \underline{\varepsilon}^{th} d\Omega \qquad 6\text{-}29$$

Now multiplying Equation 6-29 by B^T and integrating over the domain of the body and also by using Equation 6-28, we have Equation 6-30.

$$\underline{F}^{ext} = \underline{K}\underline{u} - \underline{F}^{th} \qquad 6\text{-}30$$

where, $K = \int_{\Omega} B^{T} C B d\Omega$, $F^{ext} = \int_{\Omega} B^{T} \sigma d\Omega = 0$ if there are no presence of external forces and u is the nodal displacement vector. Hence the finite element equation, Equation 6-30 is solved after applying appropriate boundary conditions to obtain nodal displacements. Once the nodal displacements are found, the strains within and element can be calculated by Equation 6-28 and the stresses can be then computed using Equation 6-27.

Thermoviscoelasticity: We develop the thermoviscoelastic analysis for the cooling cycle analogous to thermoelasticity as discussed in the previous topic based on the references (40). The viscoelastic counterpart of Equation 6-27 using the constitutive equation of viscoelasticity as given in Equation can be written as shown in Equation 6-31.

$$\underline{\sigma} = \int_{0}^{t} 2G(t-s) \frac{d(\underline{e} - \underline{e}^{th})}{ds} ds + K(\varepsilon_v - \varepsilon_v^{th})\underline{1} \qquad 6\text{-}31$$

where, e is the deviatoric strain, e^{th} is the deviatoric part of thermal which is equal to zero, ε_v is the volumetric strain, ε_v^{th} is the volumetric part of thermal strain, K is the bulk modulus and

$G(t) = G_0 \left(w_{\infty} + \sum_{i=1}^{N} w_i \exp(-t/\tau_i) \right)$ is the relaxation kernel function.

Numerical integration: To develop a recursive stress update for the constitutive Equation 6-31, we follow the similar procedure as outlined in the pressing cycle. Hence the details are

omitted. Because of the temperature dependence in the cooling cycle, we incorporate the temperature dependence in a new variable, the reduced time as given by Equation 6-32.

$$\psi = \int_0^t \frac{\tau_{ref}}{\tau\left(T(s)\right)} ds = \frac{\tau_{ref}}{A(T(s))} \qquad 6\text{-}32$$

where, τ_{ref} is the relaxation time evaluated at a suitable reference temperature, $A(T(s))$ is the shift function and $\tau = \tau_{ref}.\exp\left\{-\frac{H}{R}\left(\frac{1}{T_{ref}} - \frac{x}{T(t)} - \frac{(1-x)}{T_f(t)}\right)\right\}$ is the relaxation time given at a particular temperature.

By the midpoint integration of the stress terms we have a recursive stress update formula that can be used in the FEA implementation which is given by Equation 6-33

$$\underline{\sigma}_{n+1} = K(\varepsilon_v^{n+1} - \varepsilon_v^{(n+1)th})\underline{1} + 2G_\infty e_{n+1} + \sum_{i=1}^{N}(s_i^n)\exp\left(\frac{-\Delta\psi}{\tau_i}\right) + 2\exp\left(\frac{-\Delta\psi_{1/2}}{\tau_i}\right)G_i\Delta e \qquad 6\text{-}33$$

where, n+1 is the current load step, K is the bulk modulus, ε_v is the volumetric strain, ε_v^{th} is the volumetric part of thermal strain, G_∞, G_i are the shear modulus according to the relaxation kernel, s^n is the shear stress history variable, $\Delta e = e_{n+1} - e_n$ is the incremental deviatoric strain, τ_i is the relaxation time of the i^{th} Maxwell element and Δt is the time step. The reduced time steps are given as: $\Delta\psi = \int_{t_n}^{t_{n+1}} A(T(s))ds$ and $\Delta\psi_{1/2} = \int_{t_{n+1/2}}^{t_{n+1}} A(T(s))ds$.

Discussion: From Equation 6-25 we can see that the first stress term i.e. $K(\varepsilon_v^{n+1} - \varepsilon_v^{(n+1)th})\underline{1}$ term is the volumetric part which is elastic as we have assumed the bulk part to be elastic. The deviatoric stress term $\sum_{i=1}^{N}(s_i^n)\exp\left(\frac{-\Delta t}{\tau_i}\right) + 2\exp\left(\frac{-\Delta t}{\tau_i}\right)G_i\Delta e$ is initially zero when glass is at a temperature much higher than the transition temperature where the viscosity is of the order of

1E-6 to 1E-10 Pa.s. Hence the term $\exp\left(\frac{-\Delta t}{\tau_i}\right)$ approaches 0 and hence initially there is no accumulation of shear stress. When glass approaches the viscoelastic phase, $\tau \simeq \Delta t$, the term $\exp\left(\frac{-\Delta t}{\tau_i}\right)$ is finite. When glass is frozen to a solid the viscosity is very high i.e. of the order of 1E10 to 1E16 Pa.s and hence the term $\exp\left(\frac{-\Delta t}{\tau_i}\right)$ approaches 1 which essentially reduces the Equation 6-25 to the elastic counterpart.

CHAPTER 7
RESULTS

This chapter outlines the actual experimental molding of the lenses and the corresponding finite element simulation. The molds were designed with an aspheric profile on the lower mold and a spherical profile on the top mold. The lens corresponding to these profiles were designed at Canon Inc for commercial applications.

Two sets of molding experiments were performed. The difference between the two processes was the use of different glass materials and the corresponding molding process parameters. The same molds were used for both of the molding processes.

The results from the FEA and from the actual molding process are discussed.

Lens Molding Experiments

Mold details: The molds for the glass molding process were made of Tungsten Carbide alloy (WC) supplied by Dijet, Japan (FB01). The mold surfaces were precision ground on an ultra precision grinding machine and polished to optical quality surface finish. A very thin layer of about 80 nm of Tetrahedral amorphous Carbon (TaC) was coated on the molding surfaces of the molds. The main purpose of the coating is to reduce the friction and eradicate the sticking of the glass to the mold surfaces at the time of pressing.

The profile of the lower mold used is described by an asphere profile. Figure 7-1 shows the detailed dimensions of the lower mold. Equation 7-1 describes the asphere curve of the lower mold profile

$$z = \frac{x^2 / R}{1 + \sqrt{1 - (1+k)(x/R)^2}} + Bx^4 + Cx^6 + Dx^8 + Ex^{10} \qquad 7\text{-}1$$

where, R = 9.36599 is the radius, k = -3.36835 is the conic constant and B = 3.53073E-4, C = -5.10864E-6, D = 7.64203E-8, E = -1.19413E-9 are the asphere coefficients.

The mold has a hole at the bottom which was initially designed to house the thermocouple for better temperature measurements. However, because of machine limitations the thermocouple could not be inserted in the hole.

The profile of the upper mold is described by a spherical profile with a very small radius of curvature. Figure 7-2 shows the detailed dimensions of the upper mold. The mold material and properties are the same as the lower mold. The equation describing the spherical profile is same as shown in Equation 7-1, with radius of curvature R=54.16 and the conic constant k being 0. Also the asphere coefficients, A_i are zero.

Glass details: Two different glass materials namely P-SK57 and BK7, both manufactured by Schott Inc. were used for the two experimental glass molding processes. Schott has developed a new manufacturing process for precision gobs, which takes place in a clean environment. The precision gobs are made out of glass directly from the melt and have an overall fire-polished surface with fine surface roughness. Hence these precision gobs can be directly used for the precision molding of optical elements.

Process details: The process parameters for both the glass molding process for the different glasses are listed in Table 7-1 and Table 7-2. Figure 7-3 illustrates the process diagram for the both the molding processes.

Finite Element Simulation

Mold properties: The mechanical properties of the WC molds (lower and upper) used in the FE simulation is listed in Table 7-3. These properties were directly obtained by the manufacturer.

Glass properties: The mechanical, thermal and viscoelastic properties of P-SK57 and BK-7 used in the FE simulation are listed in Table 7-4 and Table 7-5 respectively. These properties were directly obtained from the manufacturer.

However, the structural relaxation times are a difficult parameter to obtain. It has been experimented and concluded for most of the oxide glasses, the structural relaxation time is a factor of the stress relaxation time. (41). For the particular borosilicate glass used, the factor was found to be 4. Hence the structural relaxation times used in the analysis was arrived at by multiplying the stress relaxation times by a factor of 4.

Process parameters: The process parameters used in the molding process was used in the FE simulation. Hence the process details according to Table 7-1 and Table 7-2 were used in the finite element simulation.

Results and Discussions

The results of the FE simulation of the glass molding process have been discussed here and an attempt to compare the experimental profile is made. The discussion of the results is included wherever necessary.

The two molding experiments were quite similar to each other. The only difference was the use of a different glass material in the two molding processes. Hence most of the results discussed below are similar and the results for only one of the experiments are shown. However, the final results of the molding process i.e. the residual stresses and the geometry of the deformed glass are shown for both the processes.

FE model of the assembly: Figure 7-4 shows the FE mesh of the molds and the glass assembly for the molding with P-SK 57 glass. The mesh was created using a 4 node quadrilateral element. An attempt was made to have denser mesh on sections of the periphery of glass where the mold imprint is expected. Similarly, for the mold meshing, the mold surface profiles have a denser mesh and the lower part of the mold has a relatively coarse mesh.

The assembly model for the BK-7 glass is quite similar and hence the figure is omitted. The only difference was the use of a smaller radius gob for the BK-7 molding, while the molds remained the same.

Thermal expansion of the molds: During the heating process, because of the high temperature change the profile of the mold changes due to thermal expansion. This alters the actual profile on which the glass is being molded. Figure 7-5 shows the comparison between an actual profile and the thermally expanded profile. The figure contrasts the asphere form deviation against the original form deviation which is 0 in microns.

It can be seen that for the lower mold (aspheric profile) the deviation increases from the center towards the end of the profile. The maximum deviation at the edge of the profile is about 3 microns which is quite significant deviation in precision optics.

For the upper mold profile (spherical), the deviations follow the same trend as the lower mold, but the deviations are relatively less. The maximum deviation occurs at the edge of the mold which is about 0.5 microns. This can be attributed to the fact that, since the spherical profile has a very small radius of curvature, the profile is almost flat and hence the profile deviation is less.

Deformed glass geometry: Figure 7-6 shows the deformed geometry of glass at the end of the pressing process using the P-SK57 glass and using the BK-7 glass.

The radius of the P-SK57 glass from the simulation was 4.5 mm. The radius of the experimentally measured lens was 4.61 mm. Hence the difference in the radii was less than 2%.

The radius of the BK-7 glass was 3.6 mm from the simulation. The radius of the experimentally measured lens was 3.65 mm which implies a change of less than 1.5%. Since the molds were the same, the heights of the lenses are same. Table 7-6 shows the radii of the FE

simulation and experimental lenses and the volume losses. This shows a good agreement of the FE simulation model of incompresssiblity.

Temperature distribution: There are two cooling cycles in the molding process, i.e. the initial gradual cooling and the rapid cooling. The purpose of gradual cooling is to allow uniform dissipation of heat and ensure uniform temperature distribution throughout the process so that the accumulations of residual stresses are at minimum. Figure 7-7 shows the temperature distribution at the end of gradual and rapid cooling. Because of the small size of the glass gob the temperature distribution is almost uniform for the given cooling rate.

Residual stress: The cooling process is the most critical process in the glass molding cycle. During this stage, due to non-uniform cooling and phase change of glass from viscous to elastic state, the glass develops stresses. These stresses are vital to the performance of the glass as they affect the optical qualities of the lens.

Figure 7-8 shows the 'yy' component of the residual stress at the end of the cooling process. The results predict compressive stresses near the surfaces and tensile stresses at the core. This can be attributed to the fact that the outside surface cools faster and the inner core cools relatively slower. Hence the outer surface is under compressive stresses and the inner core is in tensile stresses. Figure 7-8 also shows the residual stress for an identical glass molding process but with a higher cooling rate (twice than that shown in Table 7-1). We can see the difference in the development of residual stresses; the faster cooling rate induces higher residual stresses. The cooling rate in effect alters the point of departure from the equilibrium line. Hence faster the cooling rate, higher is the point of departure from equilibrium and hence higher residual stresses.

However, the predicted stress could not be compared with the experiments because of the unavailability of the instrument which is used to measure stresses in glass; a polarimeter. But the

results show intuitive trends and are in very good agreement with similar experimental deductions performed in by Soules, Carre and Jain (42) (43).

Shrinkage: Figure 7-9 shows the shrinkage of the glass due to the cooling process. The center bottom node was fixed to prevent rigid body motion. The final profile of the glass at end of the molding process is predicted by the profile at the end of the cooling cycle.

Profile comparison: The profile of the molded lenses was measured at MNTS using tally surf which is a diamond probe based profile measuring machine (profilometer). The experimentally measured profiles from the profilometer and the FE simulation were analyzed using Omnisurf which is a profile analysis package. The form errors were obtained as explained in the following steps.

5. The profile from the experiment/FEA was imported to omnisurf.
6. The primary asphere curve equations parameter was provided as described in Equation 7-1.
7. Then the underlying asphere curve from the imported curves was removed from the direct raw profile. The resulting form is the primary curve, which is the imported curve minus the desired form.
8. A waviness curve was fit through the primary profile which essentially was peaks and valleys using a smooth spline-Gauss function. The waviness is a measure of the low frequency error.
9. The rms error for the waviness profiles was calculated i.e. the form error

Figure 7-10 shows the form error comparison between the experimentally measured profile and the curve from the FE simulation for the asphere part of the P-SK57 lens. Figure 7-11 shows the form error comparison for the asphere part of the BK7 lens. The form errors both from the simulation and the experimental curves are less than 1 micron which is a very reasonable for the applications of precision optics. The form was analyzed only between the clear apertures of the lens which is the optically important part of the profile. However, the errors increased away from the center of the lens.

Initially, the author expected a smooth profile from the FE simulation, but as a result of the scale of comparison in microns, a smooth curve could not be obtained. The fluctuating nodal positions can be attributed to the numerical limitation of the finite element analysis. The contact constraint is imposed by a penalty parameter and the contact forces are calculated as a product of the penalty parameter and the penetrations. The penalty parameter cannot be increased beyond a certain limit as it would impair the convergence of the analysis. Hence there are always inevitably very small penetrations which are evident because of the scale of the comparison in microns. The profiles match very well in a macro sense or where the order of comparison is same as the dimensions of the geometry. However, the comparisons made here are in the order of microns and from the deviation figures, it can be seen that the deviations are less than about 1 micron (1E-3 mm). The comparisons of the FEA and the experimental deviations match reasonably well even on the scale of microns.

Table 7-7 shows the form error comparison between the asphere profiles of the P-SK57 and BK7 at the end of the process and end at the end of the pressing process. A very good agreement was observed between the root mean square errors of the profile. Obviously, as the pressing profile during the actual lens molding cannot be determined, hence the data for the experimental lens pressing profile is discarded.

Table 7-1. Process parameters for molding with P-SK-57 glass

Heating time	150 seconds
Soaking time	100 seconds
Soaking temperature	530 ºC
Pressing force	300 Newtons
Pressing time	110 seconds
Pressing temperature	530 ºC
Gradual cooling temperature	348 ºC
Gradual cooling rate	0.83 ºC/s
Rapid cooling temperature	22 ºC
Rapid cooling rate	1.63 ºC/s

Table 7-2. Process parameters for molding with BK-7 glass

Heating time	250 seconds
Soaking time	185 seconds
Soaking temperature	550 ºC
Pressing force	300 Newtons
Pressing time	120 seconds
Pressing temperature	550 ºC
Gradual cooling temperature	425 ºC
Gradual cooling rate	1.04 ºC/s
Rapid cooling temperature	20 ºC
Rapid cooling rate	1.125 ºC/s

Table 7-3. WC Fuji Alloy mold properties

Young's modulus	660000 N/mm^2
Poisson's ratio	0.22
Coefficient of thermal expansion	4.5E-6 $ºC^{-1}$

Table 7-4. P-SK57 glass properties

Physical Properties	
Young's modulus	93000 N/mm^2
Poisson's ratio	0.249
Density	3.01 g/cm^3
Radius of glass gob used	2.8 mm
Thermal Properties:	
Coefficient of thermal expansion in solid state	7.2E-6 $ºC^{-1}$
Coefficient of thermal expansion in liquid state	8.9E-9 $ºC^{-1}$
Specific heat	0.760 J/(g.K)
Thermal conductivity	1.01 W/(m.K)
Viscoelastic properties:	
Number of Maxwell elements used	1
Shear Modulus	37203
Reference temperature	593
Stress relaxation time at reference temperature	1.2757E-4
Structural relaxation time at ref. temperature	5.1028e-004

Table 7-5. BK-7 glass properties

Physical Properties	
Young's modulus	82000 N/mm^2
Poisson's ratio	0.206
Density	2.51 g/cm^3
Radius of glass gob used	2.5 mm
Thermal Properties:	
Coefficient of thermal expansion in solid state	7.1 E-6 $ºC^{-1}$
Coefficient of thermal expansion in liquid state	8.3 E-9 $ºC^{-1}$
Specific heat	0.858 J/(g.K)
Thermal conductivity	1.114 W/(m.K)
Viscoelastic properties:	
Number of Maxwell elements used	1
Shear Modulus	27516
Reference temperature	719
Stress relaxation time at reference temperature	1.4468E-4
Structural relaxation time at ref. temperature	5.7872e-004

Table 7-6. Deformed glass volume

	BK7	P-SK57
Experimental lens radius	3.65 mm	4.61 mm
FE Simulation lens radius	3.601 mm	4.5 mm
Change in radius	Less than 1.5%	Less than 2.5%

Table 7-7. Form errors of profile from FE simulation and experiment (microns, 1E-3 mm)

	Final profile		Pressing profile	
	Max. deviation	RMS	Max. deviation	RMS
P-SK57				
FE Simulation	-1.348	0.477	-1.264	.548
Experiment	0.862	0.386	x	x
BK7				
FE Simulation	0.960	0.401	1.147	0.673
Experiment	0.882	0.374	x	x

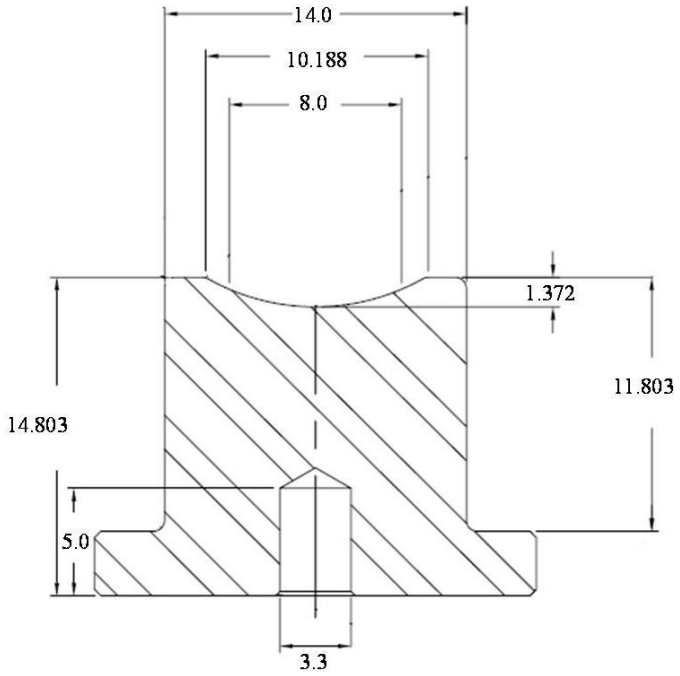

Figure 7-1. Geometry and dimensions of the lower asphere mold (mm)

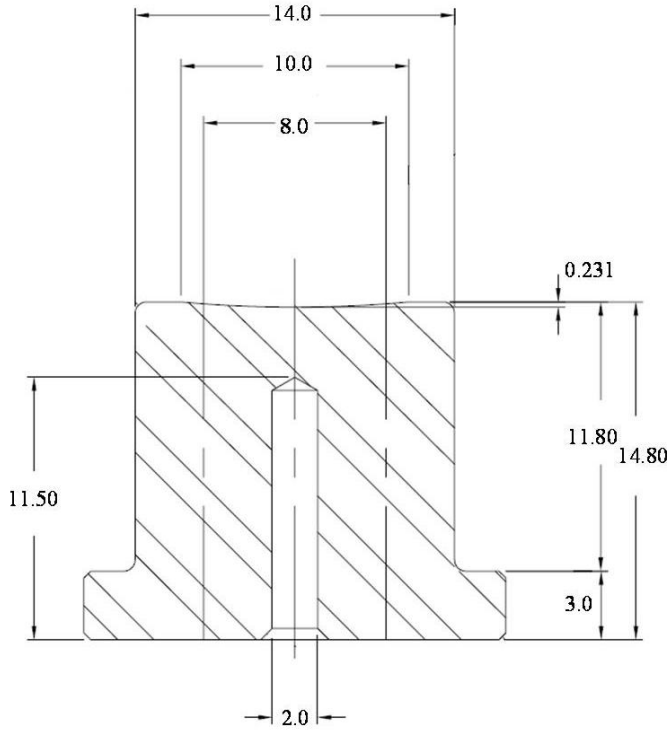

Figure 7-2. Geometry and dimensions of the upper spherical mold (mm)

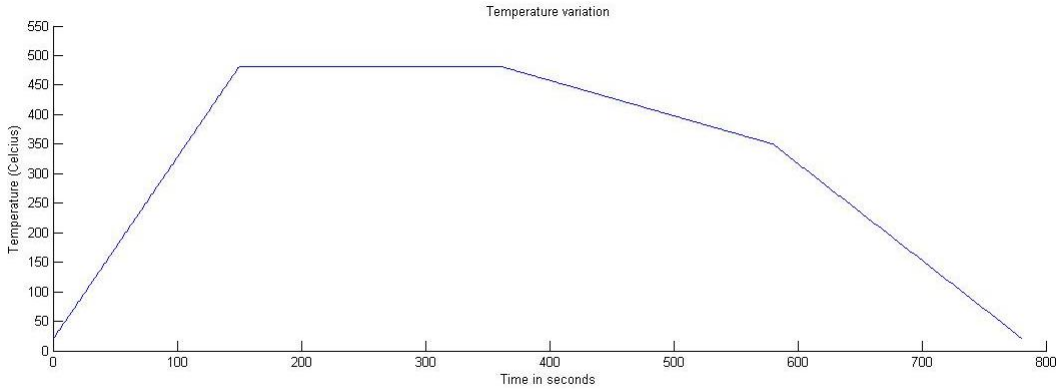

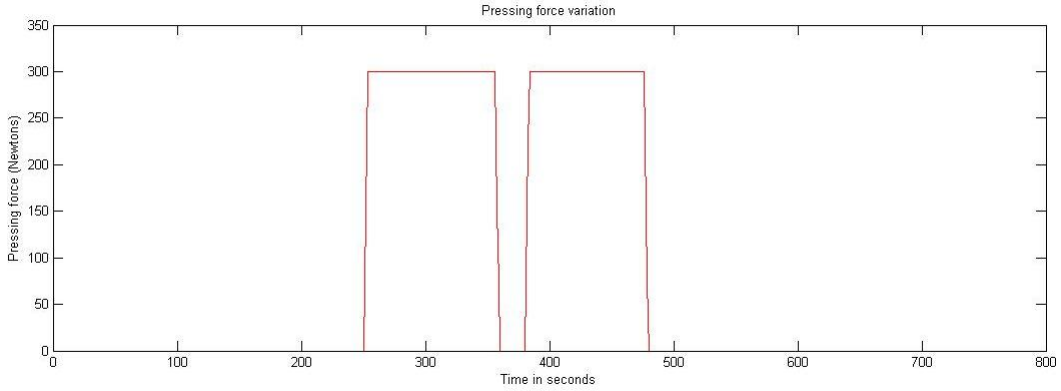

A

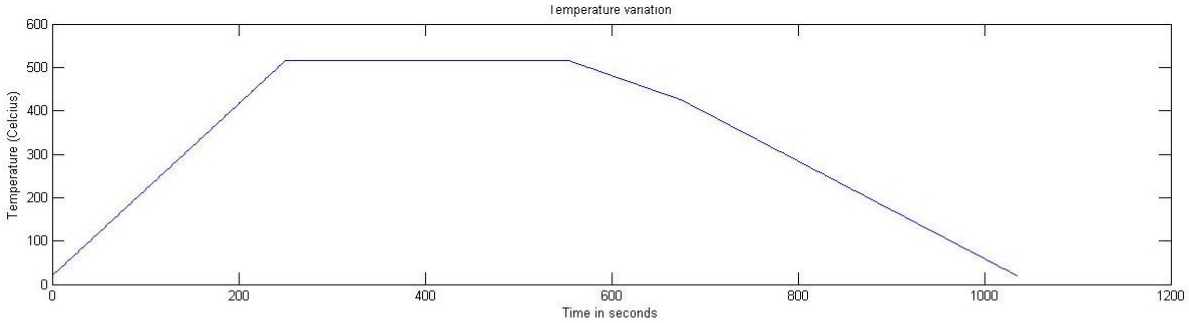

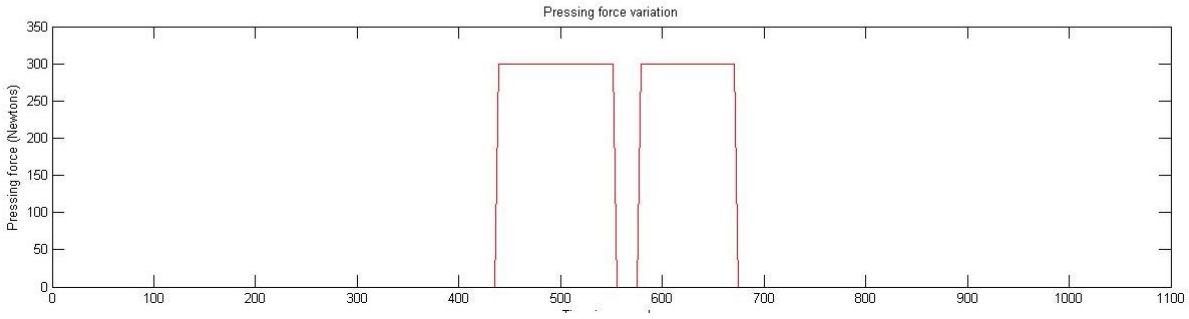

B

Figure 7-3. Process cycles for the glass molding process A)Process cycle for the P-SK57 glass molding process B)Process cycle for the BK-7 glass molding cycle

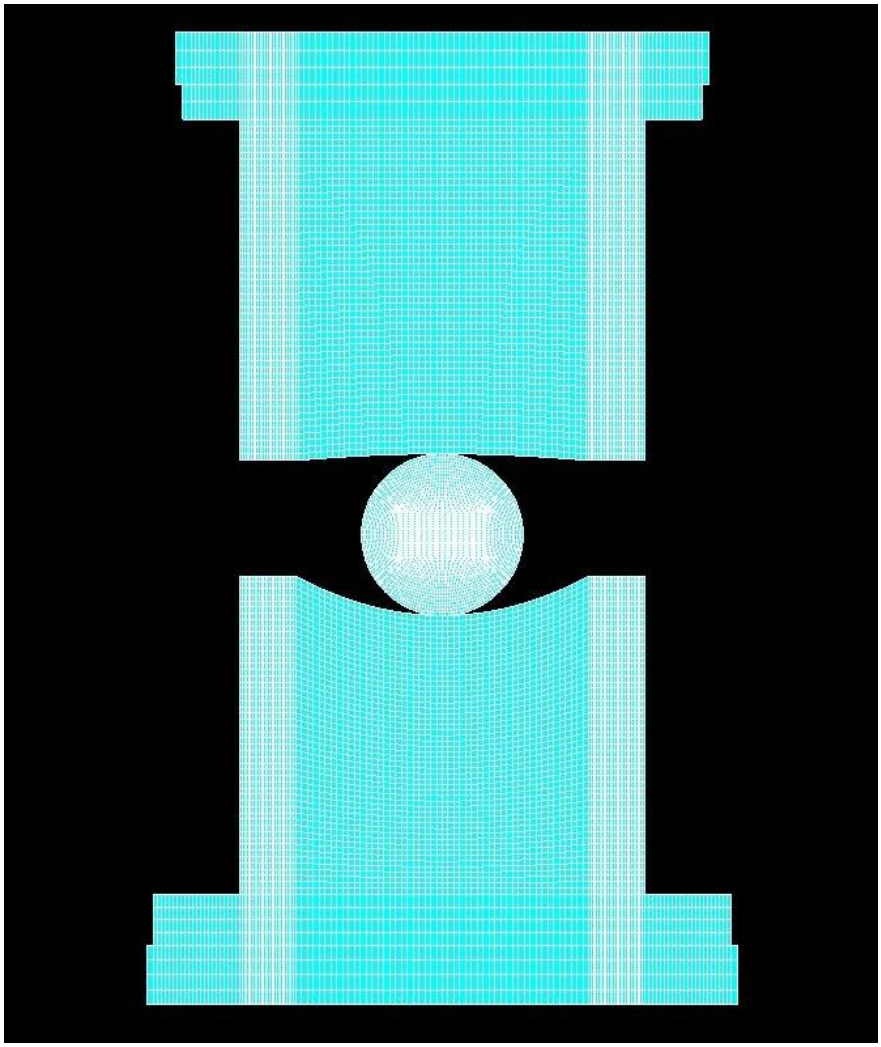

Figure 7-4. FE model of the assembly of the molds and the glass. 4 node quadrilateral elements have been used for the meshing.

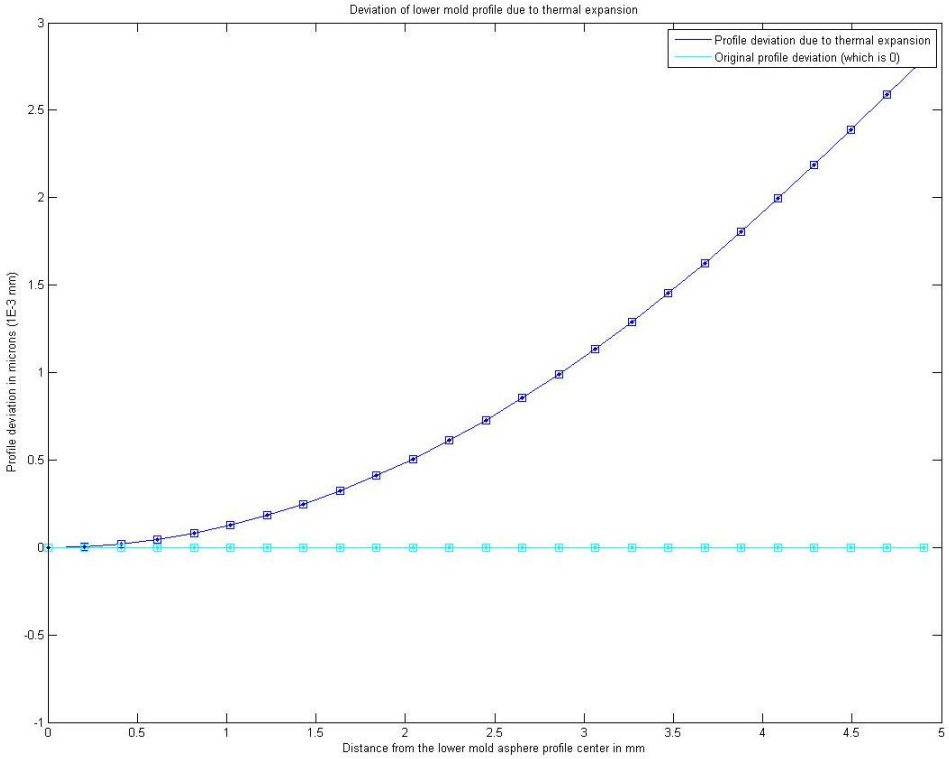

A

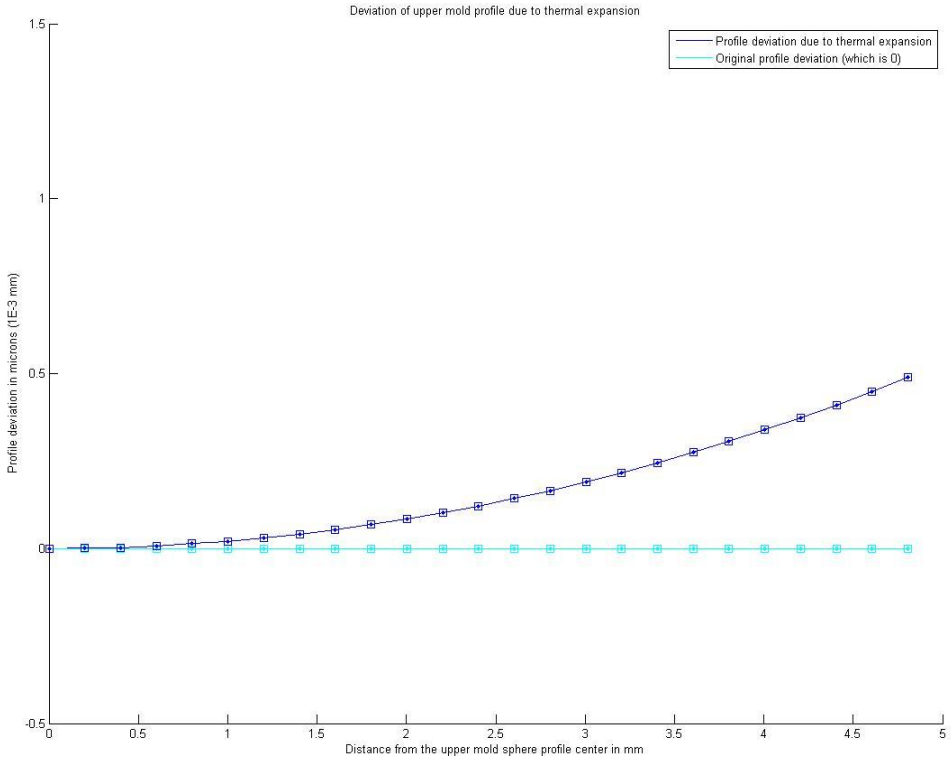

B

Figure 7-5. Thermal expansion of the lower and upper molds due to the heating cycle. A) Profile deviation of the lower asphere mold profile B) Profile deviation of the upper spherical mold profile

A

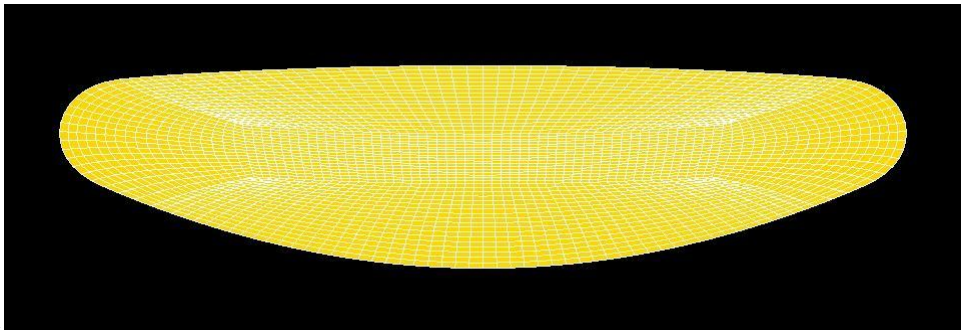

B

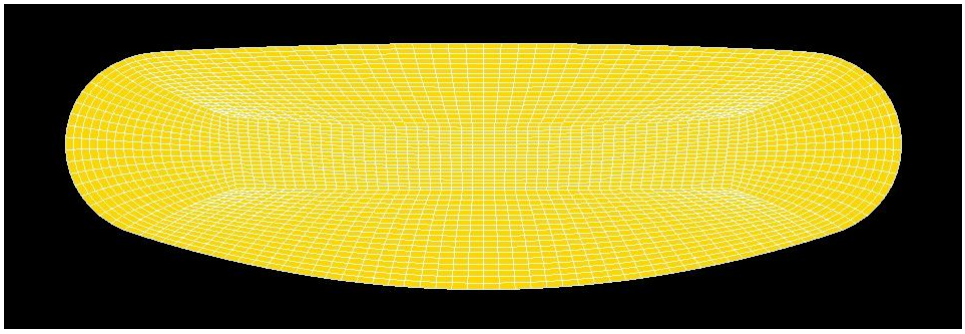

Figure 7-6. Deformed geometries of the lens at the end of the pressing process. A) Deformed geometry of the P-SK47 glass. Maximum radius from the center 4.5 mm. B) Deformed geometry of the BK-7 glass. Maximum radius from the center 3.6 mm

A

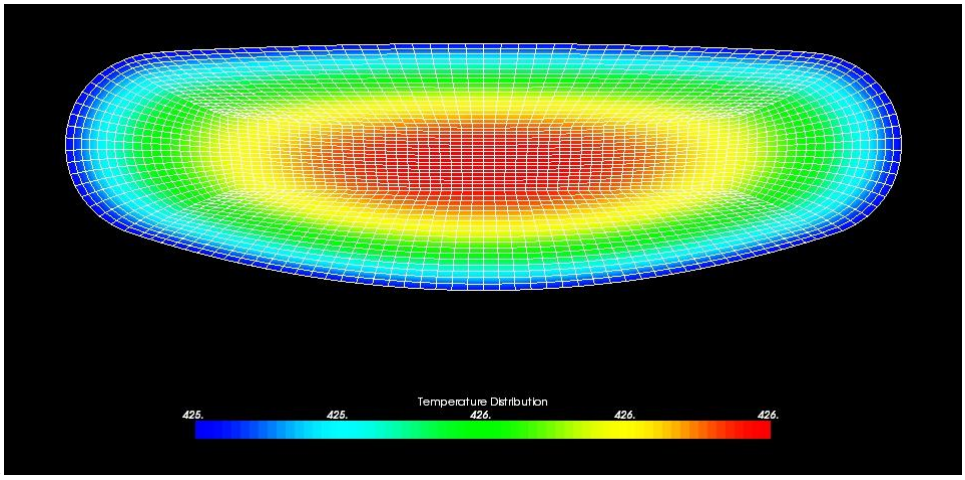

B

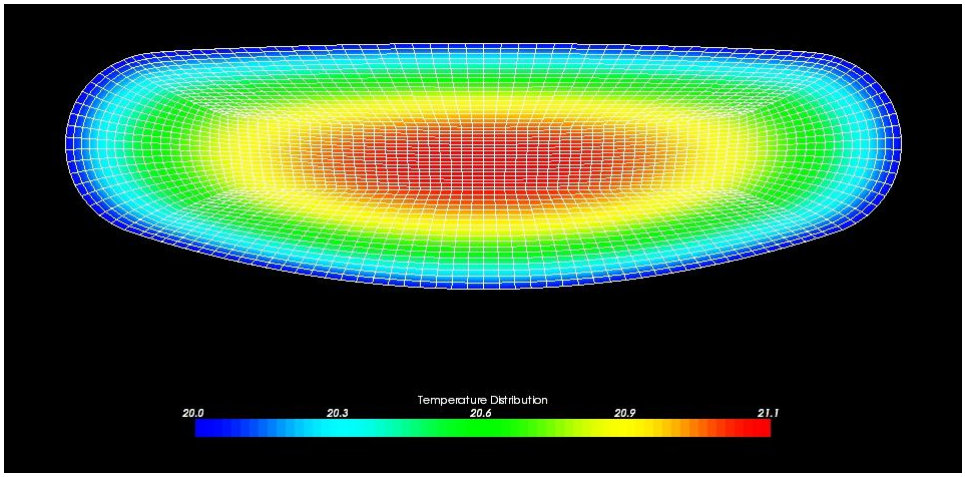

Figure 7-7. Temperature distribution at the end of cooling cycles A) Temperature distribution at the end of the gradual cooling cycle B) Temperature distribution at the end of the rapid cooling cycle

A

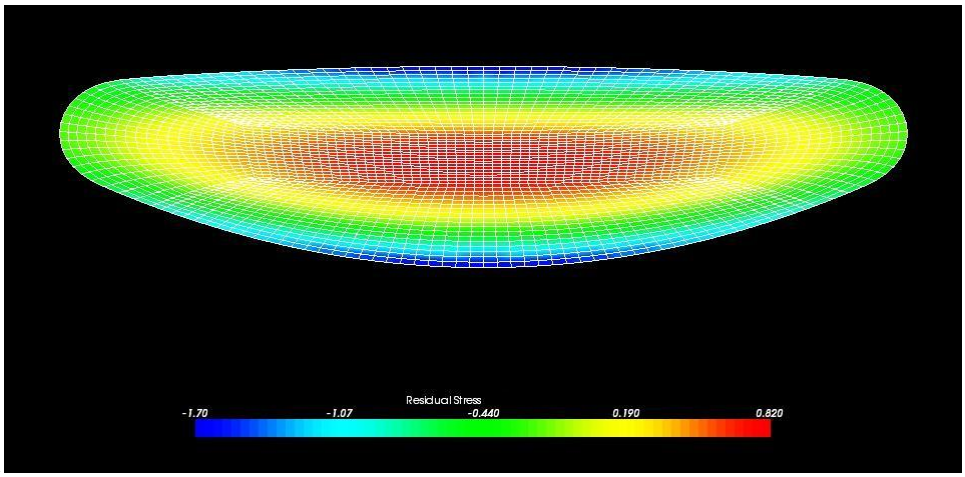

B

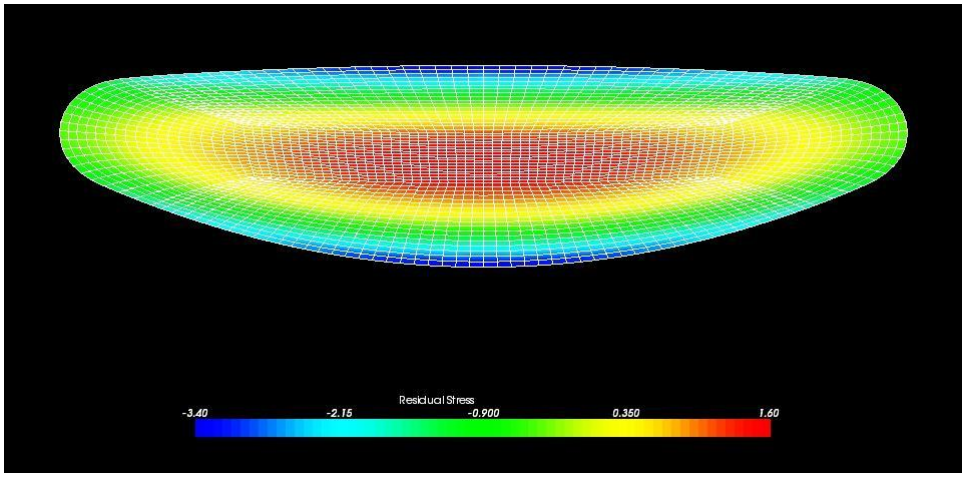

Figure 7-8. Residual stresses at the end of the molding process (MPa) A) Residual stress plot with a cooling rate of 0.83 ºC/s for the gradual cooling and 1.63 ºC/s for the rapid cooling. B) Residual stress plot with a cooling rate of 1.66 ºC/s for the gradual cooling and 3.26 ºC/s for the rapid cooling

A 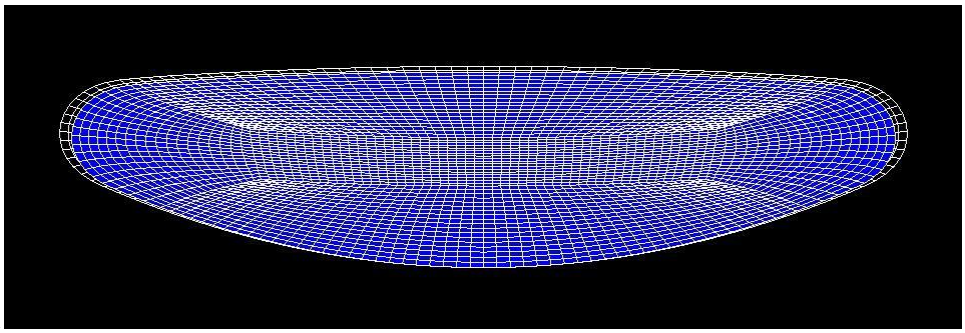

B 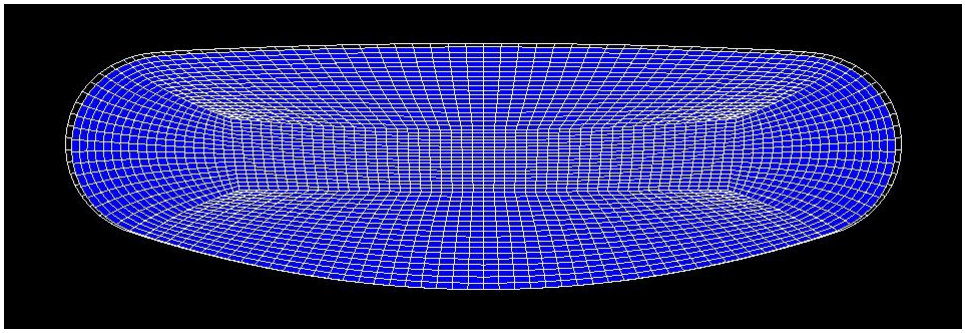

Figure 7-9. Shrinkage due to the cooling process. A) Shrinkage due to cooling for the P-SK57 molding process. B) Shrinkage due to cooling for the BK-7 molding process

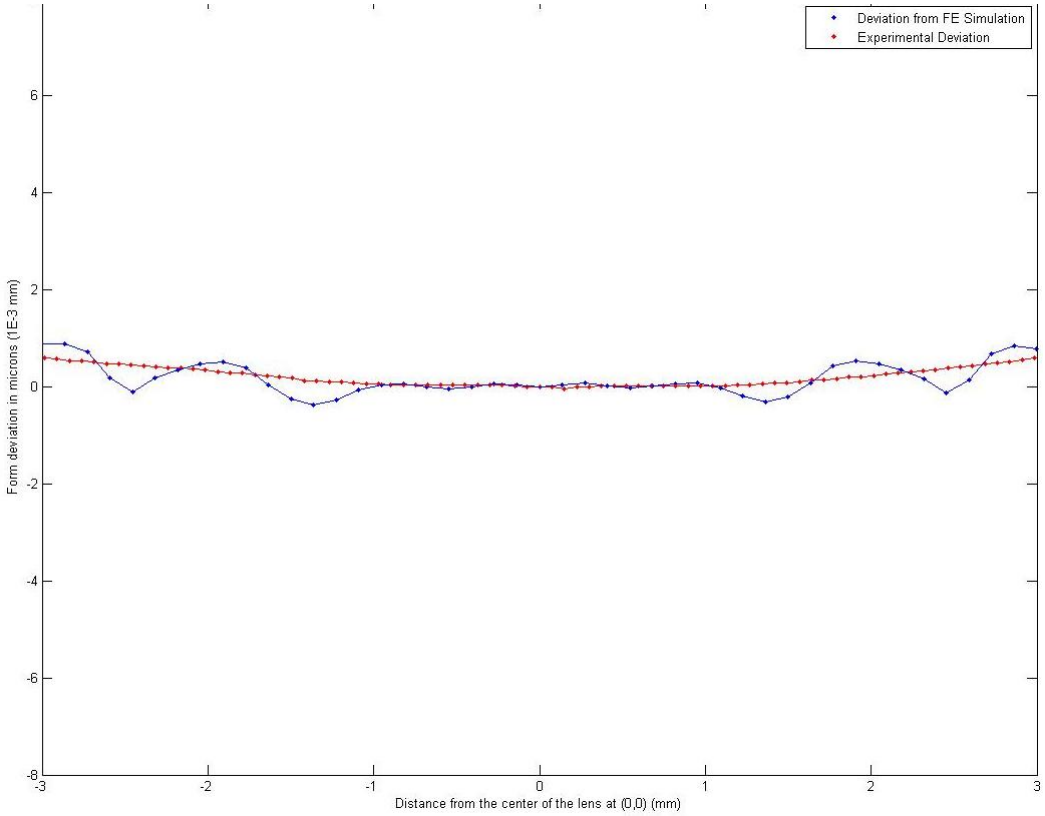

Figure 7-10. Comparisons between form errors from the actual experiment and the FEA simulation for the P-SK57 glass from the center of the lens (asphere part) (Units: 'x' axis: mm, 'y' axis: microns)

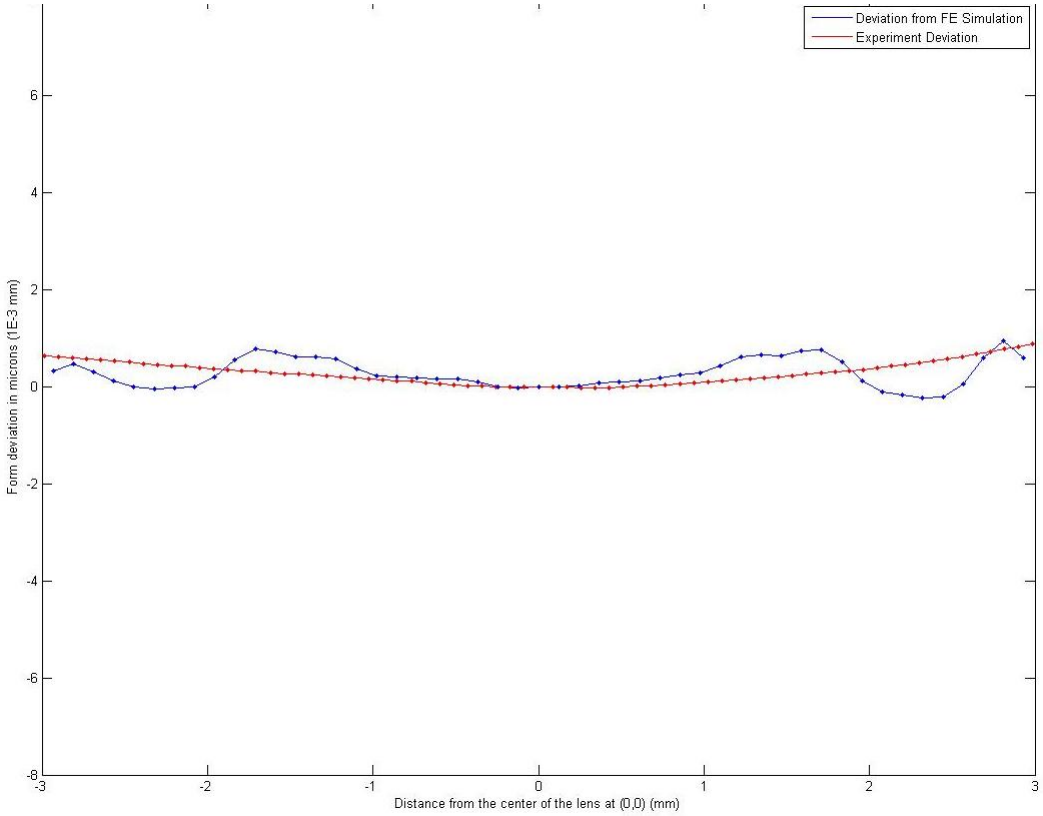

Figure 7-11. Comparisons between form errors from the actual experiment and the FEA simulation for the BK-57 glass from the center of the lens (asphere part) (Units: 'x' axis: mm, 'y' axis: microns)

CHAPTER 8
CONCLUSIONS

Summary

The primary motivation behind this research was to explore the possibility of a novel manufacturing method for the mass production of precision asphere lenses; i.e., the compression molding process. Although this process appears very much feasible, it is not adopted widely because of the thermal influences due to the high temperature molding, the behavior of glass at higher temperatures which induces residual stresses that affect the optical properties greatly. Current practice in the industry involves molding lenses using trial and error approach which is expensive and time consuming. Hence there is a need to predict the molding process and hence be able to quantify the residual stresses and the profile deviation. In this first very preliminary attempt to simulate the molding process, a relatively simplified discreet cycle by cycle analysis approach has been adopted. Important phenomena that govern the physics of glass molding process have been identified and incorporated into the modeling of the molding process. The implications of this development of a prediction tool for glass molding process in the optical fabrication industry are far stretched.

Conclusions

The results from the experimental molding show that the precision lenses can be molded within acceptable form errors. The numerical simulation of the glass molding process was performed from an engineering point of view and the results obtained were reasonably good. The residual stresses, although couldn't be verified experimentally because of limitations, was predicted which showed very good agreement with results performed in similar experiments.

The profile deviation was also predicted with reasonable accuracy. Because a smooth profile from the FE simulation was not obtained, it was not possible to calculate the change in

the aspheric coefficient directly from the FE curve. Because of the fluctuating profile from the FE, the author quantified the profile error using RMS values. A good agreement was found between the form errors from experiment and the numerical simulation.

Limitations: However, since in this first attempt there were several limitations to the development of the tool which can be dealt further to result in a more sophisticated tool. Considerations of the following factors could lead to a more sophisticated and accurate development of the tool

The thermal effects due to radiation and convection in the cooling process were neglected. They can be taken into the FE model to include heat loss due to convection and radiation. Because of lack of data from the stress relaxation tests, only 1 Maxwell element model was adopted to model viscoelasticity. Using higher number of Maxwell elements would capture the behavior of glass transition region more efficiently. The structural relaxation times are difficult to obtain and hence a factor was used for its values. As referenced before, the structural relaxation times are generally a factor of the stress relaxation times, typically lying between 4-20. All these factors may affect the calculation of residual stresses.

Because of the contact constraints and the order of profile comparisons in microns, a smooth nodal representation of the data could not be obtained. Inevitably, very small penetrations of the order of microns cause significant profile deviations. Hence, to obtain a smooth asphere curve from the FE simulation, the FE curve needs to be fitted with an asphere equation and the changes of the original asphere coefficients must be observed.

The experimentally measured profile had about 100 order of higher points that from the FE simulation. Hence the form error from the FE simulation was higher. Customizing the code to have a very high density points at the asphere part on the glass and the mold can provide a more

smooth and conformable curve to the experimental profile. The author was unable to use more than about 1800 elements on the glass and molds due to memory issues. The linear system solution algorithm was an LU factorial decomposition algorithm. For very higher system of equations, the use of a multi frontal solver or a sparse matrix solver is recommended for computational efficiency.

Future Work

This research was one of the first attempts to develop a totally standalone numerical tool dedicated to simulate the glass molding process. This development was primarily focused on the forward analysis of the problem. This tool can be reverse engineered using optimization techniques to predict the optimum mold geometry that would result in the final desirable optical profile. It can also be optimized to predict the optimum cooling profile to induce residual stresses within the acceptable limit, but yet make the manufacturing process as fast as possible.

Sensitivity analysis can be implemented which can give the user of the tool an idea about how change in different parameters affect the result of the final optical element.

In general, the progresses in numerical prediction of the glass molding process can open doors to the large volume production of precision asphere lenses. This can replace the current expensive and time consuming traditional methods. This may result in many consumer goods to be available at a cheaper and affordable rate because of the cheap production of the optical lenses which are the main reasons for the high cost.

LIST OF REFERENCES

1. Jain A, Yi A. Numerical modeling of viscoelastic stress relaxation during glass lens forming process. Journal of American Ceramic Society 2005; 88[3]: 530-535.

2. Osswald TA. Properties table. Polymer processing fundamentals; Hanser publishers; 217-226.

3. Keyworth BP, Corazza DJ, McMullin NJ, Mabbott L. Single step fabrication of refractive microlens arrays. Applied Optics 1997; 36:2198-2202.

4. Firestone GC, Jain A, Yi AY. Precision laboratory apparatus for high temperature compression molding of glass lenses. Review of Scientific Instruments 2005; 76: 063101.

5. Popovic ZD, Sprangue RA, Connell GA. Technique for monolithic fabrication of microlens arrays. Applied Optics 1988; 27: 1281-1284.

6. Yuan, Yu WX. Fabrication of refractive microlens in hybrid SiO2/TiO2 sol-gel glass by electron beam lithography. Optics Express 2003; 11: 899-903.

7. Jacobs SD. Innovations in polishing of precision optics. International Progress on Advanced Optics and Sensors 2003; 3-14.

8. Maschmeyer RO, Andrysick CA, Geyer TW, Meissner HE, Parker CJ, Sanford LM. Precision molded glass optics. Applied Optics 1983; 22: 2413-2415.

9. Menden-Piesslinger GA, Ven de Heuvel JH. Precision pressed optical components mode of glass and glass suitable therefor. US Patent 4391915.

10. Uhlmann DR, Kreidl NJ. Glass science and technology. Academic Press Inc. 1986; 3: chapter 4.

11. Sadegh N, Vachtsevanos GJ, Barth EJ, Pirovolou EJ, Smith MH. Modeling the glass forming process. Glass Technology 1997; 38[6]: 216-218.

12. Krishna A, Harper BD, Lee JK, Finite element viscoelastic analysis of temperature and moisture effects in electronic packaging. Transactions of the ASME 1995; 117: 192-200.

13. Rekhson SM, Thermal stresses, relaxation, and hysteresis in glass. Glass Science and Technology, Journal of American Ceramic Society 1993; 76[5]: 1113-1123.

14. Cuong PD, Bruggemann D. Optimizing the cooling parameters for annealing of glass bottles by stress simulation according to the viscoelasticity theory. Glass Science Technology 2005; 78[4]: 141-145.

15. Hoque A, Fischer CE, Wu WT. Simulation of the glass pressing process using 2-dimensional large deformation finite element software. Scientific Forming Technologies Corporation, Ohio, USA. Paper #353.

16. Soules TF, Robert FB, Rekhson SM, Markovsky A. Finite-element calculation of stresses in glass parts undergoing viscous relaxation. Journal of American Ceramic Society 1987; 70[2]: 90-95.

17. Jain A, Yi AY, Numerical simulation of compression molding of aspherical glass lenses. American Institute of Physics 2004; 0-7354-0188-8/04

18. McCrum NG, Buckley CP, Bucknell CB. Principles of Polymer Engineering 2003; 117-176.

19. Malvern LE. Introduction to the mechanics of a continuous medium. Prentice Hall Publications 1977; Chapter 4.

20. Simo JC, Hughes TJ. Computational inelasticity. Springer-Verlag Berlin and Heidelberg GmbH & Co. K 1998; Chapter 10.

21. The IUPAC Compendium of Chemical Terminology. Glass transition temperature 1997; [66].

22. Scherer GW. Relaxation in glass and composites. Wiley-Interscience Publication 1986; Chapter 1: 1-15.

23. Schott Optical Glass Catalogue North America Inc. 2000.

24. Jain A, Firestone GC, Yi AY. Viscosity measurement by cylindrical compression for numerical modeling of precision lens molding process. Journal of American Ceramic Society 2005; 88[9]: 2409-2414.

25. Scherer GW. Relaxation in glass and composites. Wiley-Interscience Publication 1986; Chapter 9: 113-130.

26. Narayanaswamy OS. A model of structural relaxation in glass. Journal of The American Ceramic Society 1971; 54[10]: 491-498.

27. This has often been called the Williams-Watts function since those authors used I in 1970. However, this function has been applied in studies of creep and stress relaxation dating back to Kohlrausch (1847). It was studied extensively by Debast and Gilard and was first used in conjunction by Mazurin et al. (1975). Hence it seems inappropriate to attach any individual's name.

28. Scherer GW. Relaxation in glass and composites. Wiley-Interscience Publication 1986; Chapter 5: 56-66.

29. Schwarzl F, Staverman AJ. Time-temperature dependence of linear viscoelastic behavior. Journal of Applied Physics 1952; 23: 838-43.

30. Tool AQ, Relation between inelastic deformation and thermal expansion of glass in its annealing stage. Journal of The American Ceramic Society 1946; 29[9]: 240-253.

31. Johnson AR, Quigley CJ. A viscohyperelastic Maxwell model for rubber viscoelasticity. Rubber Chemistry and Technology 1992; 65[1]: 137-153.

32. Chen T. Determining a prony series for a viscoelastic material from time varying strain data. U.S. Army Research Laboratory 2000; NASA/TM-2000-210123.

33. Madapusi S, Kim NH. Predictive molding of precision glass optics. SAE World Congress Detroit 2009; 09B-0258.

34. Simo JC. On fully three-dimensional finite strain viscoelastic damage model: Formulation and computational aspects. Computational Methods in Applied Mechanics 1987; 60: 153-173.

35. Taylor RL, Pister KS, Goudreas GL. Thermomechanical analysis of viscoelastic solids. International Journal for Numerical Methods in Engineering 1970; 2: 45-49.

36. Structures with material nonlinearities – viscoelasticity, ANSYS Theory Manual.

37. Structures with material nonlinearities – large deformation viscoelasticity, ANSYS Theory Manual.

38. Hughes TJ. The finite element method linear static and dynamic finite element analysis. Prentice Hall Inc. 1987.

39. Markovsky A, Soules TF. An efficient and stable algorithm for calculating fictive temperatures. Journal of The American Ceramic Society 1984; 67[4]: C-56-C-57.

40. Simo JC, Hughes TJ. Computational inelasticity. Springer-Verlag Berlin and Heidelberg GmbH & Co. K 1998; Chapter 10.

41. Scherer GW. Relaxation in glass and composites. Wiley-Interscience Publication 1986; Chapter 10: 139-145.

42. Carre H, Daudeville L. Numerical simulation of soda line silicate glass tempering. Journal De Physique 1996; 6: C-175-C1-185.

43. Jain A. Experimental study and numerical analysis of compression molding process for manufacturing precision aspherical glass lenses. PhD thesis 2006. The Ohio State University.

BIOGRAPHICAL SKETCH

Shriram was born in Chennai, India. He was raised primarily in New Delhi, India. In June 2006, he earned a Bachelor of Technology degree in mechanical engineering from New Delhi. He joined the MDO research group under the guidance of Dr. Nam-Ho Kim in August 2007 as a Master of Science student.